Journal of Theoretical Biology 474 (2019) 25–41

Contents lists available at ScienceDirect

Journal of Theoretical Biology

journal homepage: www.elsevier.com/locate/jtb

The formation of the Thickveins (Tkv) gradient in Drosophila wing discs: A theoretical study

Zhan Chen

Department of Mathematical Sciences, Georgia Southern University, Statesboro, GA, United States

ARTICLE INFO

Article history:
Received 24 April 2018
Revised 6 February 2019
Accepted 12 April 2019
Available online 15 April 2019

Keywords:
Drosophila wing disc
Dpp signaling
Tkv
Brk
Patterning
Mathematical model

ABSTRACT

The development of the wing imaginal disc (wing disc) is commonly adopted for the studies of patterning and growth which are two fundamental problems in developmental biology. Decapentaplegic (Dpp) signaling regulates several aspects of wing development, such as the anterior (A)-posterior (P) patterning, cellular growth rate, and cell adhesion. The distribution and activity of Dpp signaling are controlled in part by the expression level of its major type I receptor, Thickveins (Tkv). In this paper, we focus on theoretically investigating mechanisms by which the highly asymmetric pattern of Tkv is established in Drosophila wing discs. To the end, a mathematical model of Hh signaling and Dpp signaling is proposed and validated by comparisons with experimental observations. Our model provides a comprehensive view of the formation of Tkv gradients in wing discs. We found that engrailed (En), Hedgehog (Hh) signaling, and Dpp signaling cooperate to establish the asymmetric gradients of Tkv and pMad in the wing disc. Moreover, our model suggests a Brinker-mediated mechanism of Dpp-dependent repression of Tkv. Based on this mechanism, a couple of predicted experimental observations have been provided for further lab confirmation.

1. Introduction

Drosophila melanogaster, the common fruit fly, is one of the most widely used model organisms in biology (Hamaratoglu et al., 2014). Many fundamental biological, neurological, and physiological properties are highly conserved between mammals and Drosophila, and nearly 75% of human disease-associated genes are believed to have a functional homolog in the fly (Pandey and Nichols, 2011). Therefore, a better understanding of the underlying mechanisms of developmental processes in Drosophila may further our knowledge of similar processes in other organisms including humans. The fly can be used not only for primary small molecule discovery but also in the drug discovery process due to its attractive features such as very low comparative cost, powerful genetics, and highly conserved disease pathway (Pandey and Nichols, 2011). In particular, the development of the wing imaginal disc (wing disc) is commonly adopted for the studies of patterning and growth, which are two fundamental problems in developmental biology. Although sophisticated genetic networks are available in the Drosophila wing disc, in many cases it remains unclear how these networks interact and cooperate to form observed spatiotemporal patterns of gene expression, and then control the overall phenotypes of organs such as the wing (Umulis and Othmer, 2015).

The decapentaplegic (Dpp) signaling pathway is one of the most important and extensively studied pathways for both patterning and growth in the wing disc (Hamaratoglu et al., 2014; Tabata and Takei, 2004). It regulates several aspects of wing development, such as the anterior-posterior patterning, cellular growth rate, and cell adhesion (Doumpas et al., 2013). Dpp is induced by Hedgehog (Hh) and is a member of the Bone Morphogenetic Protein (BMP) subfamily. Ligand Dpp is expressed and secreted in a stripe of anterior cells adjacent to the AP boundary. After their secretion, Dpp molecules transport and form a concentration gradient that determines cell fates in a concentration-dependent manner (Umulis and Othmer, 2015). Through Dpp binding with its receptors, preferentially with type-I receptor Thickveins (Tkv), local extracellular concentration of Dpp is converted into the intracellular gradient of phosphorylated Mothers Against Dpp (pMad), which is considered as the sole known transmitter of Dpp-Tkv activity to regulate its downstream target gene expressions (Restrepo et al., 2014; Tanimoto et al., 2000). Moreover, Dpp plays a necessary role in the growth of wing disc (Hamaratoglu et al., 2014). Both the Dpp gradient and its cellular response (visualized by pMad antibodies) expand and adjust to the growing tissue size (Restrepo et al., 2014; Ben-Zvi et al., 2011). However, how Dpp coordinates patterning

E-mail address: zchen@georgiasouthern.edu

https://doi.org/10.1016/j.jtbi.2019.04.015
0022-5193/

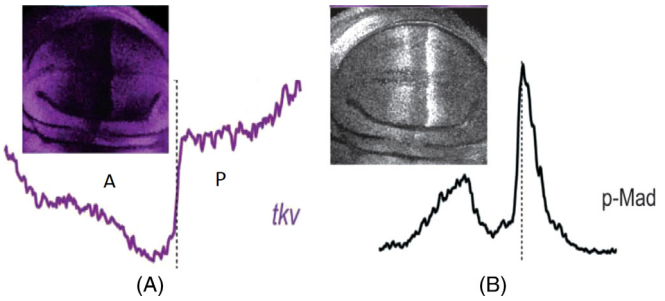

Fig. 1. Confocal microscopy images of *tkv* expression and pMad gradients which were taken from previous work by Tabata and Takei (2004) (A) Experimental measurement of *tkv* expression (Tabata and Takei, 2004); (B) Experimental measurement of pMad (Tabata and Takei, 2004). For the image of wing disc in the upper left corner of (A), the intensity of pink color reflects the intensity of *tkv* level which can be translated into the underneath curve of *tkv* concentration along A-P axis. Similarly, in the image of wing disc in the upper left corner of (B), the lightness quantifies the level of pMad which can be described by the underneath curve of pMad concentration.

and growth during development is not understood (Restrepo et al., 2014).

The distribution and activity of Dpp signaling are controlled in part by the expression level of its major type I receptor, Thickveins (Tkv). Dpp binds to its receptor to form a ligand-receptor complex which in turn phosphorylates Mothers against Dpp to form pMad. The level of pMad is considered as an indicator of the Dpp signaling activity. Removal of Tkv function leads to the absence of pMad while ubiquitous expression of Tkv elevates pMad everywhere in the disc and causes disc overgrowth (Tanimoto et al., 2000). The profile of *tkv* expression shows an intricate pattern in the wing disc (See Fig. 1(A))(Tabata and Takei, 2004). It displays the lowest level in cells of the Hh signaling region, and the Tkv level gradually gets higher away from the AP boundary in the A compartment. It also increases sharply in the cells abutting the AP border before a much slower increase toward the periphery in the P compartment. Furthermore, the *tkv* concentration climbs sharply in the peripheral regions of both A and P compartments, and the level of *tkv* is higher in the P compartment than that in the A compartment.

Partially due to the highly asymmetrical profile of Tkv in the wing disc (Tanimoto et al., 2000), the pattern of Dpp signaling activity represented by the pMad level is also complicated (See Fig. 1(B)). The level of pMad is not directly proportional to the Dpp concentration. In the P compartment, it is highest in cells near the AP boundary where the Dpp concentration is high, and it decreases sharply in a short distance. In the A compartment, the pMad level is hyperrepressed in cells adjacent to the AP boundary where both Hh and Dpp levels are high, and then becomes higher away from the AP boundary and forms the second steep gradient.

Intensive studies on the Dpp signaling have given us some understanding of the formation of Tkv. As shown theoretically and experimentally (Chen and Zou, 2018; Funakoshi et al., 2001; Tanimoto et al., 2000; Lecuit and Cohen, 1998), the Tkv distribution is dynamically regulated by En, Hh signaling, and Dpp signaling. Firstly, it was found that both Hh and En act through master of thickveins (Mtv), a transcription factor, to control the tkv expression (Funakoshi et al., 2001; Tanimoto et al., 2000). En positively regulates Tkv in the P compartment by downregulating the *mtv* expression. As such, the upregulation of the Tkv level by En results in the sharp jump of pMad across the AP boundary and the highest peak of pMad in the cells abutting to the AP boundary (Chen and Zou, 2018). Secondly, Hh negatively modulates Tkv in cells of Hh signaling area by upregulating the mtv expression. Thirdly, it was postulated that Dpp negatively regulates Tkv and thereby expands the spatial range of its own activity (Tanimoto et al., 2000; Tabata and Takei, 2004; Lecuit and Cohen, 1998).

However, how Dpp signaling affects Tkv distribution has not been understood yet. Our previous work suggests that Dpp does not repress Tkv directly (Chen and Zou, 2018). It has been experimentally observed that the repression of *tkv* expression by Dpp may involve one of Dpp target genes optomotor blind (*omb*) (Umulis and Othmer, 2015; del Álamo Rodrıguez et al., 2004). Therefore, Dpp-dependent repression of Tkv is most likely in an indirect manner through Dpp downstream transcription factor or target genes. Regarding the Dpp downstream signaling, the pMad gradient in the wing disc leads to the concentration dependent repression of BMP transcription factor, Brinker (Brk). It was found that pMad of sufficiently large concentration can downregulate the level of gene *brk* expression (Moser and Campbell, 2005). Otherwise, the presence of Brk protein is required to repress the *brk* regulation by medium pMad level. Meanwhile, the Brk protein can negatively regulate the *brk* expression in lateral regions in the absence of pMad (Moser and Campbell, 2005; Restrepo et al., 2014). Consequently, the *brk* expression is high in the peripheral (or lateral) regions of wild-type wing disc, and there is no expression in the central (medial) areas. The level of *brk* is graded between lateral and medial areas (Moser and Campbell, 2005).

Indeed, a large portion of Dpp-dependent transcriptional regulation is mediated by Brk. Brk often represses Dpp target genes. For instance, the repression of *brk* causes the activation of other two target genes, spalt (sal) and omb (Bangi and Wharton, 2006) which are directly repressed by Brk at different levels. In particular, sal is completely repressed by lower levels of Brk, and thus it has a narrower expression domain than omb (Moser and Campbell, 2005; Bangi and Wharton, 2006). Moreover, most of the growth regulation by Dpp signaling can be attributed to Brk (Doumpas et al., 2013).

In this work, we focus on theoretically exploring the underlying mechanisms of the pattern formation of the Tkv gradient in Drosophila wing discs. To the end, we extend a previous baseline mathematical model in which several critical experimental observations were integrated (Chen and Zou, 2018; Funakoshi et al., 2001; Tanimoto et al., 2000; Tabata and Takei, 2004; Lecuit and Cohen, 1998). The previous model of the AP patterning was able to capture major features of complex profiles of *tkv* expression and pMad in both anterior and posterior regions of the wing disc. it can also be used to examine specific roles of En, Hh, and Dpp on the formation of Tkv and pMad gradients. Nonetheless, the previous model is not able to reproduce the graded increase of *tkv* expression in the peripheral regions of both A and P compartments by using a direct Dpp-dependent repression term (Chen and Zou, 2018). Therefore, it remains unclear how the Dpp signaling downregulates the Dpp receptor Tkv, and how the graded level of Tkv is established in the peripheral regions.

One of our objectives is to obtain a comprehensive view of the establishment of the Tkv gradient in the wing disc. For this purpose, we hypothesize that the Dpp-dependent repression of Tkv is also mediated by Brk: Dpp represses *brk* expression via pMad, and Brk upregulates Tkv. As such, a novel description of the dynamical formation of *brk* expression is incorporated into our model together with a new impact term of Brk on Tkv. To validate the current model, we test the computational spatial profiles of *tkv* expression, pMad, and *brk* expression against experimentally-measured results. An important test is to determine whether the model enables us to completely reproduce the highly asymmetrical patterns of *tkv* expression and pMad throughout the disc. Furthermore, specific roles of En, Hh and Dpp in the establishment of the complex Tkv gradient will be investigated and a new light will be shed on the formation of Tkv gradients.

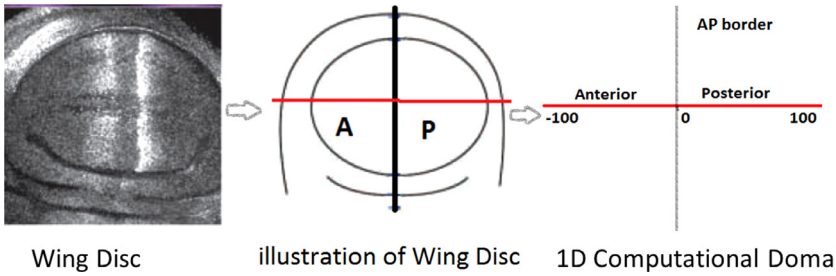

Fig. 2. Simplified view of the wing disc as a one-dimensional (1D) system (Chen and Zou, 2018). The left two figures are taken from Tabata and Takei (2004) with some revisions. It is reasonable to consider wing discs in Drosophila as a two-dimensional (2D) system since they are approximately flat tissues; Moreover, the 2D system can be further simplified into a one-dimensional (1D) system due to the fact that from all positions along the AP boundary the patterning of species is similar.

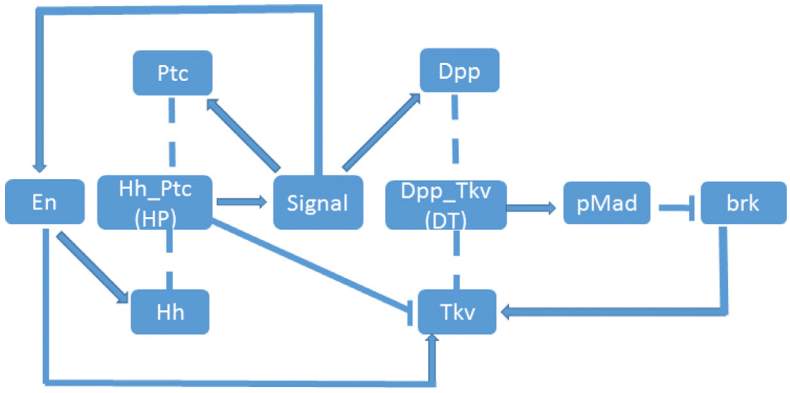

Fig. 3. A network flow of Anterior-Posterior patterning of the Drosophila wing disc in which dotted lines represents ligand-receptor binding to form a complex. For example, Dpp and Tkv bind to form Dpp-Tkv complex. This network flow is based on several experimental observations and facts: Engrailed (En) induces the Hh expression in the P compartment: ligand Hh and its receptor Ptc form Hh-Ptc complex to activate the Hh signaling (Nahmad and Stathopoulos, 2009); Hh signaling induces the *dpp* and *ptc* expression near the AP boundary in the A compartment (Tabata and Takei, 2004); Tkv is a preferred receptor of Dpp in the wing disc (Funakoshi et al., 2001; Tanimoto et al., 2000); Hh signaling is found to repress Tkv levels near the AP boundary and the level of Tkv can be upregulated by En (Funakoshi et al., 2001); Dpp binds Tkv to phosphorylate Mothers Against Dpp (pMad); Moreover, we hypothesize that Dpp signaling represses the Tkv level through Brk which upregulates Tkv (Bangi and Wharton, 2006; Moser and Campbell, 2005; Umulis and Othmer, 2015).

2. Mathematical model and computational methodology

2.1. Simplified view of the wing disc

We modeled the patterning of wing disc in a one-dimensional (1D) system. The reasoning is as follows: Because wing discs (left of Fig. 2) in Drosophila are approximately flat tissues, it is reasonable to consider them as a two-dimensional (2D) system (middle of Fig. 2). Moreover, from all positions along the AP boundary, Hh fluxes across the A compartment and Dpp transports in both A and P compartments. Therefore, the 2D system can be further simplified into a 1D system (right of Fig. 2). In our 1D computational domain, the AP boundary is considered to divide the whole computational domain equally into anterior and posterior compartments.

2.2. Mathematical model

The present model is formulated according to a proposed simple interaction network (See diagram Fig. 3) which integrates several existing experimental findings: Engrailed (En) induces the Hh expression in the P compartment; Hh and its receptor Ptc form the Hh-Ptc complex to activate the Hh signaling (Nahmad and Stathopoulos, 2009); Hh signaling induces dpp, ptc and en gene expressions near the AP boundary in the A compartment (Tabata and Takei, 2004); Tkv is a major type I receptor of Dpp in the wing disc (Funakoshi et al., 2001; Tanimoto et al., 2000); Hh signaling is found to repress the Tkv level near the AP boundary and the level of Tkv can be upregulated by En (Funakoshi et al., 2001); Dpp binds Tkv to phosphorylate Mothers Against Dpp (pMad). PMad directly represses *brk* expression. Moreover, the Tkv level can be repressed by the Dpp signaling (Bangi and Wharton, 2006; Moser and Campbell, 2005; Umulis and Othmer, 2015; Winter and Campbell, 2004; del Álamo Rodrıguez et al., 2004; Umulis and Othmer, 2015). The Dpp-dependent repression of Tkv is hypothesized to be mediated by protein Brk which positively regulates Tkv. For simplicity, the level of pMad is assumed to be linearly proportional to the level of Dpp-Tkv complex ($\overline{DT}$). This assumption is inspired by experimental observations that the absolute number of occupied receptors is linearly proportional to the level of nuclear Smad protein (Tanimoto et al., 2000; Shimizu and Gurdon, 1999). As such, by using the Dpp-Tkv complex level to represent the pMad level, we don't need to explicitly compute pMad.

Our proposed model consists of two modules according to the interacting Hh and Dpp signaling networks shown in Fig. 3. We used a one-dimensional (1D) system (See Fig. 2 in the Section 2.1) to describe the AP patterning of wing disc (Nahmad and Stathopoulos, 2009; Lander et al., 2002). Computationally, the total length of the AP axis is set to be 200 μm. The original point is regarded as the AP boundary which equally divides the whole domain into anterior ($[-100, 0)$) and posterior ($(0,100]$) compartments (Chen and Zou, 2018; Irons et al., 2010; Nahmad and Stathopoulos, 2009; Umulis and Othmer, 2015; Lander et al., 2002; Kicheva et al., 2007). Moreover, since the formation of morphogen gradients is much faster than cell proliferation (Kicheva et al., 2007), it is reasonable to assume that discs have a fixed size for our study (Chen and Zou, 2018). The Hh module, involving Hh, Ptc and $\overline{HP}$, was originally formulated in our previous work (Chen and Zou, 2018). For completeness, it is described in Algorithm A.1. Meanwhile, a new extended Dpp module, which involves the dynamic of *brk* expression and Brk-mediated regulation of Tkv, is

described in the following:

$$\frac{\partial[Dpp]}{\partial t} = D_{dpp}\frac{\partial^2[Dpp]}{\partial x^2} + \alpha_{sigdpp}\frac{[Signal]^d}{(M_{dpp})^d + [Signal]^d} - k_{dt}^{+}[Dpp][Tkv] + k_{dt}^{-}[\overline{DT}] \quad (1)$$

$$\frac{\partial[\overline{DT}]}{\partial t} = k_{dt}^{+}[Dpp][Tkv] - k_{dt}^{-}[\overline{DT}] - \beta_{dt}[\overline{DT}] \quad (2)$$

$$\frac{\partial[Tkv]}{\partial t} = \alpha_{tkv} + (1-a(x))\alpha_{enp} + \alpha_{ena}\frac{\left(\frac{[\overline{HP}]}{[Ptc]}\right)^{ne}}{(M_{en})^{ne} + \left(\frac{[\overline{HP}]}{[Ptc]}\right)^{ne}} - r_{hhtkv}\frac{\left(\frac{[\overline{HP}]}{[Ptc]}\right)^{nh}}{(M_{hp})^{nh} + \left(\frac{[\overline{HP}]}{[Ptc]}\right)^{nh}} + \alpha_{bt}\frac{[brk]^{nb}}{M_{brk}^{nb} + [brk]^{nb}} - k_{dt}^{+}[Dpp][Tkv] + k_{dt}^{-}[\overline{DT}] - \beta_{tkv}[Tkv] \quad (3)$$

$$\frac{\partial[brk]}{\partial t} = \alpha_{brk} - r_{pmd}\left\{\frac{[\overline{DT}]}{dp}(H([\overline{DT}]) - H([\overline{DT}] - dp)) \times H(T_{brk}[brk] - bl) + H([\overline{DT}] - dp)\right\} - r_{brk}T_{brk}[brk] - \beta_{brk}[brk] \quad (4)$$

where $[Dpp]$, $[Tkv]$, $[\overline{DT}]$, and $[brk]$ are concentrations of Dpp, free Tkv protein, the Dpp-Tkv complex and gene *brk*, respectively. Involved $[\overline{HP}]$, [Ptc] and [Signal] are calculated by equations in the Hh module (A.1) representing concentrations of the Hh-Ptc complex, Hh receptor Ptc and Hh signaling activity, respectively. The first two equations of Dpp and $[\overline{DT}]$ are inherited from our previous work (Chen and Zou, 2018). D_{dpp} is the effective diffusion coefficient of Dpp; k_{dt}^{+} represents the association coefficient of the Dpp-Tkv complex; k_{dt}^{-} is for the dissociation coefficient. Also, a(x) is a characteristic function of the A compartment in which $a(x) = 1$ in the A compartment and $a(x) = 0$ in the P compartment. In addition, the Dpp degradation in the wing disc is described in the formula of Dpp-Tkv complex $\overline{DT}$ in Eq. (2). $\alpha_{sigdpp}\frac{[Signal]^d}{(M_{dpp})^d+[Signal]^d}$ models the induction rate of Dpp by Hh signaling.

The equation of free Tkv protein has been extended and revised in the present work. One modification is that we introduced the upregulation of Tkv by En in Hh signaling cells. Another is that the repression of Tkv by Dpp signaling has been changed from using a direct Dpp-dependent repression term into an upregulation term by Brk. As done in our previous work (Chen and Zou, 2018), a constant rate is used for ubiquitous activation or induction, and Hill functions for activation or regulation with a threshold. Specifically, α_{tkv} is the ubiquitous activation rate of Tkv. α_{enp} represents the induction rate of Tkv by En in the P compartment (Tabata and Takei, 2004; Funakoshi et al., 2001). Moreover, the downregulation rate of *Tkv* by the Hh signaling is taken into consideration by subtracting a Hill function $\frac{r_{hhtkv}(\frac{[\overline{HP}]}{[Ptc]})^n}{(M_{tkv})^n+(\frac{[\overline{HP}]}{[Ptc]})^n}$ (Tabata and Takei, 2004; Funakoshi et al., 2001) where it is assumed that the repression depends on the ratio of Hh-Ptc complex and Ptc concentrations (Casali and Struhl, 2004). In addition, $\alpha_{ena}\frac{(\frac{[\overline{HP}]}{[Ptc]})^{ne}}{(M_{en})^{ne}}$ is added to consider the promotion of Tkv by En in the A compartment where En is induced by the Hh signaling. Finally, the repression of Tkv by Dpp is described by the term $\alpha_{brk}\frac{brk^{nb}}{M_{brk}^{nb}+brk^{nb}}$. Here we assume that brk positively regulates the level of Tkv according to the network flow. Note that in Eq. (3), we imposed a parameter constraint $\alpha_{tkv} - r_{hhtkv} > 0$ to guarantee that the net activation rate of Tkv is always biologically positive even in the presence of Hh repression. The positivity of the Tkv concentration at steady state has been shown in A.3.

Moreover, we integrated a few experimental observations to formulate the dynamic of gene *brk* in Eq. (4) (Moser and Campbell, 2005). In the equation, $H(x)$ is the heaviside function in which $H(x) = 1$ when $x > 0$ and $H(x) = 0$ if $x < 0$. Also T_{brk} is the indicator of the presence of Brk protein (Moser and Campbell, 2005). $T_{brk} = 1$ indicates normal transcription of *brk* or the presence of Brk protein. $T_{brk} = 0$ shows the absence of Brk protein. For the positive or negative regulation of brk expression, $Rep([\overline{DT}]) = r_{pmd}\{\frac{[\overline{DT}]}{dp}(H(\overline{DT}) - H([\overline{DT}] - dp))H(T_{brk}[brk] - bl) + H([\overline{DT}] - dp)\}$ is used to describe the repression of brk by the level of pMad which is represented by the concentration of $\overline{DT}$. If $[\overline{DT}] > dp$, the function term $Rep([\overline{DT}]) = r_{pmd}$. It reflects the sufficient repression of brk by a high enough level of pMad concentration in medial regions (Moser and Campbell, 2005); When $0 < [\overline{DT}] < dp$ and $T_{brk} = 1$, $Rep([\overline{DT}]) = r_{pmd}\frac{[\overline{DT}]}{dp}$. This results in the graded brk in mediolateral regions in the presence of Brk protein (Moser and Campbell, 2005). Furthermore, The Brk protein can negatively regulate the level of gene *brk* (Moser and Campbell, 2005; Restrepo et al., 2014) which

Table 1
Parameter values for the Hh module.

Symbol	Description	Value	Reference
D_{hh}	Hh diffusion coefficient	0.5 μm²/s	Nahmad and Stathopoulos (2009); Kicheva et al. (2007); Chen and Zou (2018)
α_{hh}	Hh maximal activation rate	3.4×10^{-3} μMs^{-1}	Nahmad and Stathopoulos (2009)
α_{Ptc}	Ptc maximal activation rate	9.8×10^{-5} μMs^{-1}	Chen and Zou (2018)
α_{sigptc}	Signal induction rate	6.9×10^{-4} μMs^{-1}	Chen and Zou (2018)
α_{signal}	Signal maximal activation rate	1.6×10^{-4} μMs^{-1}	Nahmad and Stathopoulos (2009)
β_{hh}	Hh degradation rate	3.3×10^{-3} s^{-1}	Nahmad and Stathopoulos (2009)
β_{Ptc}	Ptc degradation rate	1.5×10^{-3} s^{-1}	Nahmad and Stathopoulos (2009)
β_{hp}	Hh-Ptc complex degradation rate	1.5×10^{-3} s^{-1}	Nahmad and Stathopoulos (2009)
β_{signal}	Signal degradation rate	5.5×10^{-4}s^{-1}	Nahmad and Stathopoulos (2009)
k_{hp}^{+}	Hh-Ptc association rate	7.15×10^{-2} μM^{-1}s^{-1}	Lander et al. (2002); Nahmad and Stathopoulos (2009)
k_{hp}^{-}	Hh-Ptc de-association rate	0 s^{-1}	Nahmad and Stathopoulos (2009)
M_{Ptc}	Ptc half-maximal activation	0.14 μM	Chen and Zou (2018)
M_{signal}	Signal half-maximal activation	2.135	Nahmad and Stathopoulos (2009)
p	Hill coefficient (Ptc)	3	Nahmad and Stathopoulos (2009)
s	Hill coefficient (Signal)	6.8	Nahmad and Stathopoulos (2009)

Table 2
Some parameter values for the Dpp signaling module.

Symbol	Description	Value	Reference
D_{dpp}	Dpp Diffusion	0.3 $\mu m^2/s$	Kicheva et al. (2007); Lander et al. (2005); Teleman and Cohen (2000)
β_{dt}	Dpp-Tkv complex degradation rate	2.52×10^{-4} s^{-1}	Lander et al. (2002, 2005); Kicheva et al. (2007)
k_{dt}^{+}	Dpp-Tkv association rate	0.1 μ M^{-1} s^{-1}	Lander et al. (2002); Nahmad and Stathopoulos (2009)
$[Dpp]_{\max}$	maximum level of Dpp	0.9 μM	Kicheva et al. (2007)
$[Tkv]_{\max}$	maximum level of Tkv	0.34 μM	Nahmad and Stathopoulos (2009); Lander et al. (2002)
α_{sigdpp}	dpp maximal activation rate	2×10^{-4} μMs^{-1}	Chen and Zou (2018)
α_{tkv}	Tkv production rate	8.57×10^{-5} μMs^{-1}	Chen and Zou (2018)
α_{brk}	brk production rate	3×10^{-5} μMs^{-1}	This work
α_{enp}	Engrailed dependent production rate	2.74×10^{-5} μMs^{-1}	Chen and Zou (2018)
α_{ena}	Engrailed dependent production rate	2.74×10^{-5} μMs^{-1}	Chen and Zou (2018)
α_{bt}	Brk dependent upregulaton rate	2.2×10^{-5} μMs^{-1}	this work
r_{hhtkv}	Hh maximal repression rate	3.43×10^{-5} μMs^{-1}	Chen and Zou (2018)
r_{pmd}	pMad maximal repression rate	3×10^{-5} μMs^{-1}	This work
r_{brk}	brk self repression rate	1.2×10^{-4} μMs^{-1}	This work
β_{tkv}	Tkv degradation rate	2.52×10^{-4} s^{-1}	Chen and Zou (2018)
β_{brk}	brk degradation rate	3×10^{-5} s^{-1}	Chen and Zou (2018)
k_{dt}^{-}	Dpp-Tkv de-association rate	0.0067 s^{-1}	Chen and Zou (2018)
M_{dpp}	Dpp half-maximal activation	0.05 μM	Ayers et al. (2010)
M_{en}	En half-maximal activation	4.2	Nahmad and Stathopoulos (2009); Chen and Zou (2018)
M_{hp}	$\frac{HP}{Ptc}$ half-maximal repression	2.135	Nahmad and Stathopoulos (2009)
M_{brk}	brk half-maximal activation	0.15 μM	This work
d	Hill coefficient (Dpp)	3	Nahmad and Stathopoulos (2009)
nh	Hill coefficient (Tkv)	3.4	Nahmad and Stathopoulos (2009)
ne	Hill coefficient (En)	1	This work
nb	Hill coefficient (brk)	6	This work
dp	pMad repression threshold	0.05 μM	This work
bl	Brk presence threshold	0.01 μM	This work

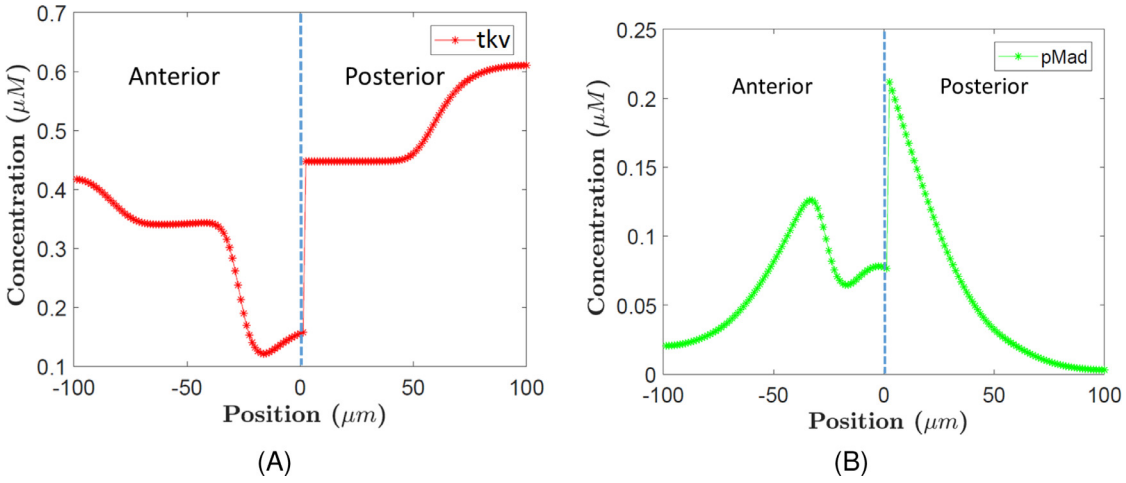

Fig. 4. Numerical results of *tkv* expression and pMad gradients by current model completely capture the features of experimentally-observed Tkv and pMad patterning in (A): numerical profile of gene *tkv* expression; (B): Numerical profile of pMad; Our numerical patterns match the experimental observations (See Fig. 1) very well. Both of them completely capture the features of *tkv* and pMad patterning. Regarding the *tkv* distribution, it clearly displays the lowest *tkv* expression in the Dpp expression region, and the level of *tkv* gets higher away from the AP boundary in both A and P compartments. Moreover, the basal level of *tkv* is higher in the P compartment than that in the A compartment. Furthermore, the *tkv* level increases sharply in the peripheral regions of both A and P compartments. To display the level of *tkv* expression, we used the total concentration of protein Tkv which consists of free and bound Tkv proteins. For the pMad profile, firstly, the level of pMad is low in the Hh expression area despite high levels of Dpp. Secondly, there exist two concentration steep gradients. The lower peak is located away from the AP boundary and the higher peak occurs abutting to the AP boundary in the P compartment.

is described in the term $r_{brk}T_{brk}[brk]$. Here r_{pmd} is the maximum repression rate. We set r_{pmd} equal to α_{brk} in this work due to the fact there is no *brk* in the middle region where the Dpp signing itself sufficiently repress brk. By doing so, the net activation rate of *brk* and the concentration of *brk* can be always biologically positive. Moreover, *dp* is for the threshold value of $[\overline{DT}]$ to sufficiently repress brk by pMad itself, and *bl* is the lowest concentration of Brk which can trigger pMad's repression on Brk.

2.3. Computational methodology

More than 20 parameters, such as effective diffusion coefficients, binding parameters, and degradation rates, are involved in the present model. A base set of parameter values used in our simulations is listed in the Tables 1 and 2 for the Hh and Dpp signaling modules, respectively. Although the involved parameters are not precisely known, their reasonable range can be estimated according to *in vitro* experimental measurements, biacore binding data, and other existing related resources. In Appendix A.4, supporting literature and evaluating processes are given in detail for chosen parameter values. Moreover, the parameter sensitivity analysis in the Appendix A.5 can demonstrate the robustness of our model against parameter changes within a certain range.

Initial conditions for all species or complexes are set to be zero before the onset of the system except for *Ptc* (Strigini and Cohen, 1997). This is supported by an experimental result that

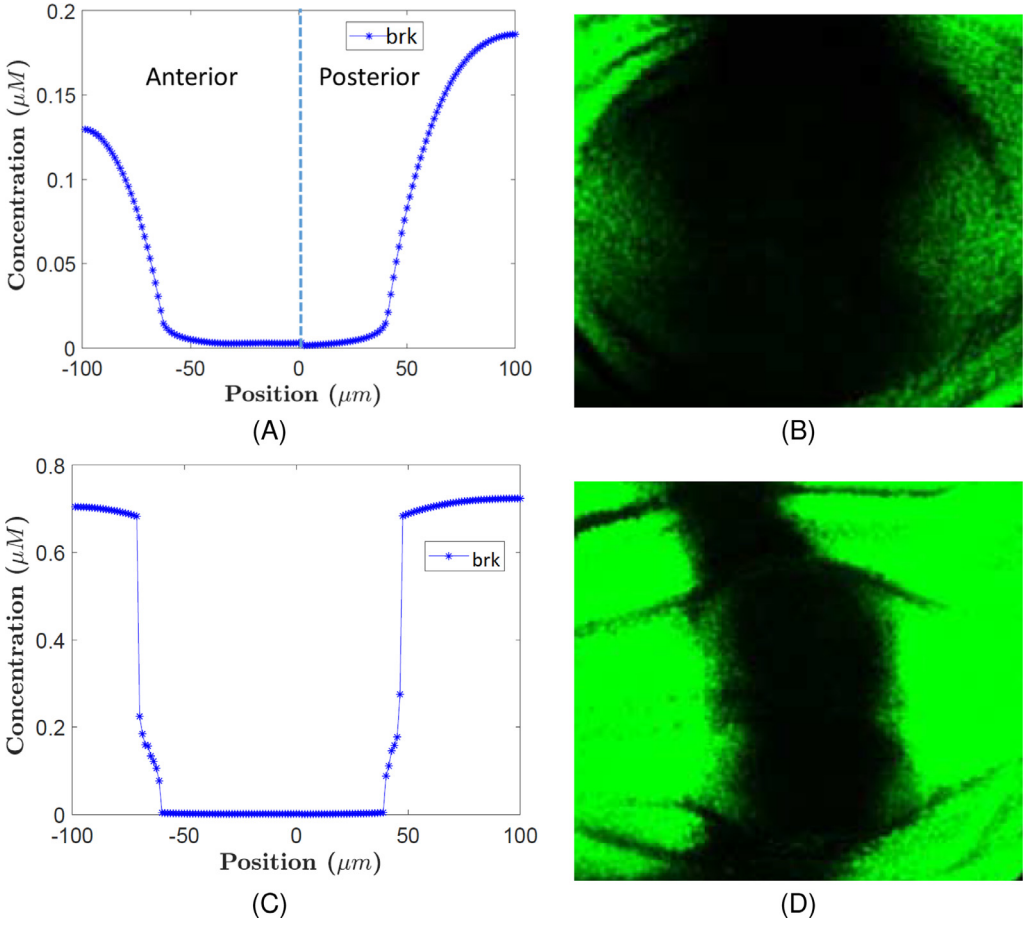

Fig. 5. In both wild-type and mutant cases, our numerical patterns of *brk* expression match experimental measurements conducted by Moser and Campbell in their previous work (Moser and Campbell, 2005). (A) Computational profile of wild-type *brk*; (B) Experimental observation for a phenotypically wild-type disc where the intensity profile of *brk* expression is displayed in green color (Taken from Fig. 6(A) of the paper (Moser and Campbell, 2005)); (C) Computational profile of *brk* when Brk is mutant; (D) Experimental observation with mutant Brk where the intensity profile of *brk* expression is displayed in green color (Taken from Fig. 6(B) of the paper (Moser and Campbell, 2005)). It is seen that our numerical result fits the pattern of wild-type *brk* well. The *brk* expression is high in the periphery (or lateral) regions of wild-type wing disc, and there is no expression in the central (medial) areas. The level of *brk* is graded between lateral and medial areas (Moser and Campbell, 2005). However, it is seen that the graded *brk* expression found in wild-type discs is lost in the mutant. Moreover, there is a fairly sharp boundary between high levels of expression laterally/mediolaterally and no expression medially. Our numerical result also captures the loss of the graded *brk* expression as well as the dramatic increase of *brk* level mediolaterally in the Brk mutant. Note that as described in the Moser's paper (Moser and Campbell, 2005), the imaginal discs shown here were analyzed by optical XZ sections. Confocal Z-section series were collected on a Bio-Rad Radiance 2000 confocal microscope and were subsequently processed using the Object Image program to generate intensity profiles and optical XZ sections. More experimental details can be found in the paper for interested readers. (For interpretation of the references to colour in this figure legend, the reader is referred to the web version of this article.)

the wild-type patterning can be sufficiently rescued when one re-initializes the system artificially with [Hh]=0 (Chen and Zou, 2018; Strigini and Cohen, 1997). For the initial condition of Ptc, it is set as previously (Nahmad and Stathopoulos, 2009; Chen and Zou, 2018):

$$[Ptc](x,0) = \frac{a(x)\alpha_{Ptc}}{\beta_{Ptc}} \tag{5}$$

In addition, zero-flux is set as boundary conditions (B.C.) of mobile morphogens Hh and Dpp at $x = \pm 100$ μm (Chen and Zou, 2018). That is a good approximation because the ranges of both Hh and Dpp gradients are short compared to the size of each compartment. Our model system was numerically solved using MATLAB. In particular, a MATLAB ODE solver ode15s, which is a variable-step and variable-order solver, was adopted for solving the system of differential equations. Also, the central finite difference scheme was used to discretize Lagrangian diffusion terms, and nonlinear terms were evaluated by previous-time-step values. All of results shown in this paper were computed with 160 grid points until the steady state was reached. Note that the same numerical patterns were obtained with finer mesh such as 320 and 640 grid points.

3. Numerical results

3.1. Model validation by wild-type profiles of tkv expression, pMad, and brk expression

In this section, numerical profiles of Tkv and Dpp signaling activities generated by the present model will be compared with experimental measurements. Completion of these comparisons will validate the model and justify our further analysis. A key test is to determine whether the highly asymmetric pattern of *tkv* expression can be reproduced throughout the whole wing disc. In addition to the Tkv profile, another significant checkpoint will be whether the resulting pMad pattern which is the indicator of Dpp signaling strength will perfectly match the experimental measurement. Finally, the computational profiles of downstream transcription factor *brk* will be compared with counterpart experimental images.

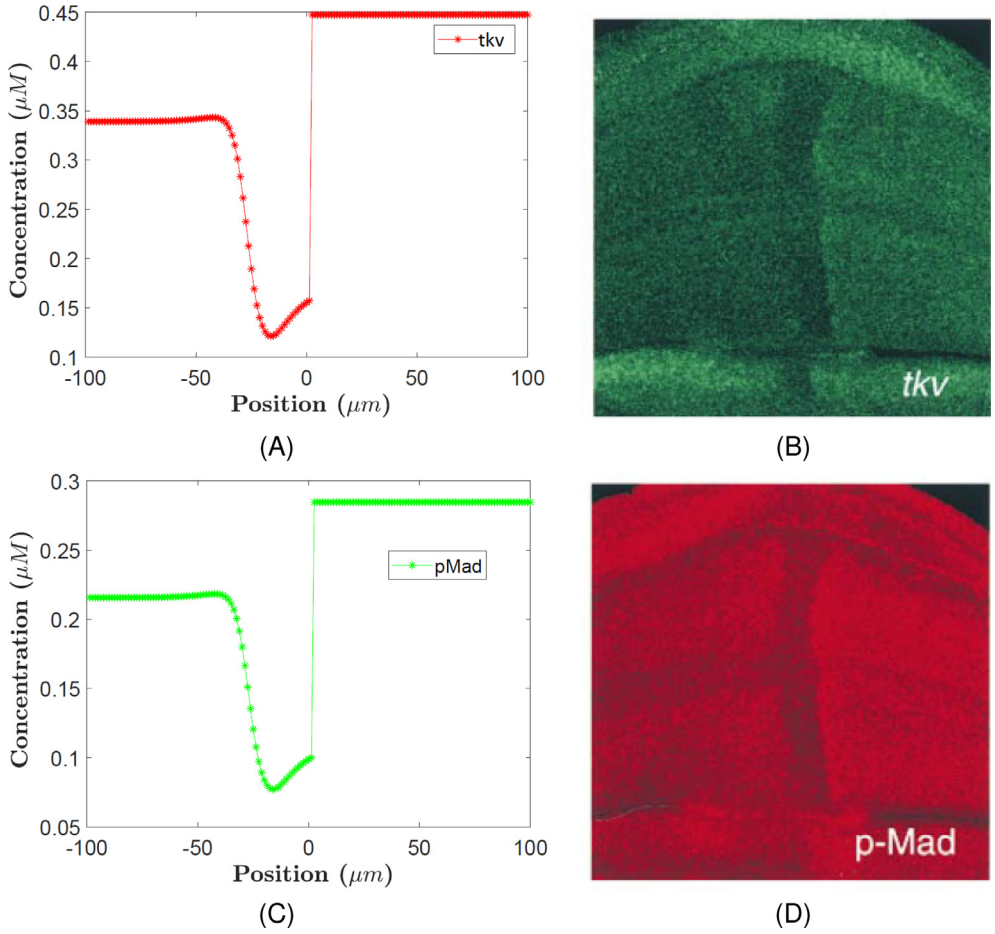

Fig. 6. In the presence of excess dpp expression, our numerical patterns of *tkv* expression and pMad fit the experimental observations performed by Tanimoto et al. in their previous work (Tanimoto et al., 2000). (A) Computational profile of *tkv* expression; (B) Experimental image of *tkv* expression (Tanimoto et al., 2000) in the disc that ubiquitously express dpp in which the lightness of green color reflects the intensity of *tkv* expression level; (C) numerical profile of resulting pMad; (D) Experimental image of pMad measurement in the disc (Tanimoto et al., 2000) where the lightness of red color reflects the magnitude of pMad level. Note that (B) and (D) are taken from Fig. 5(B) of the paper (Tanimoto et al., 2000). It shows that our numerical predictions are consistent with the experimental outcomes and captures all dramatic changes due to excess Dpp. Note that as described in the Tanimoto's paper (Tanimoto et al., 2000), all imaginal discs shown in this figure were stained with appropriate antibodies wing. To monitor reporter gene expression, Immunofluorescent images were observed on a Zeiss confocal laser microscope 510. More experimental details can be found in the paper by Tanimoto et al. (For interpretation of the references to colour in this figure legend, the reader is referred to the web version of this article.)

3.1.1. Tkv and pMad profiles

To display the level of *tkv* expression, we used the concentration of total Tkv protein which consists of free and bound Tkv proteins. Because it has been shown that the concentration of *tkv* expression is proportional to the level of total Tkv protein at the equilibrium state (See details in the Algorithm A.2). It turns out that our proposed model is able to reproduce complex patterns of Tkv and pMad throughout the whole computational domain. First of all, the numerical profile of gene *tkv* expression shown in Fig. 4(A) matches the experiment in Fig. 1 (A) very well, and it captures all of its features: 1. The level of Tkv greatly increases across the AP boundary from the A compartment to the P compartment; 2. Tkv concentration is higher in the basal region (between the periphery and the AP boundary) of the P compartment than that in the A compartment; 3. The concentration of Tkv in the A compartment is lowest a few cell diameters away from the AP boundary and gets higher away from the Dpp secretion region; 4. The level of Tkv clearly climbs from the basal to peripheral regions of both A and P compartments. Moreover, the 1D numerical profile of resulting pMad also perfectly fits the experiments (Fig. 4(B) vs Fig. 1(B)). Note that for simplicity, the level of pMad is represented by the Dpp-Tkv complex level $[\overline{DT}]$ under a reasonable assumption that the pMad level is linearly proportional to the level of Dpp-Tkv complex (Tanimoto et al., 2000; Shimizu and Gurdon, 1999).

3.1.2. Pattern of brk expression

In our model, transcription factor Brinker is used as a mediator of the Dpp-dependent repression of Tkv. Therefore, it is important to have an experimentally comparable Brinker profile produced by our model. Generating the Brinker gradient is a complicated process which involves the incorporation of the repression by pMad, self-repression by Brk protein, and the presence of Brk (Moser and Campbell, 2005). It turns out that our numerical prediction of *brk* expression is consistent with the experimental observations. The numerical and experimental patterns of *brk* expression can be seen in Fig. 5(A) and (B), respectively. For the wild-type pattern, the *brk* expression is high in the lateral regions, and there is no expression in the medial areas. Also, the level of *brk* is graded between lateral and medial regions. The comparison with wild-type profiles, in turn, justify our *brk* equation.

3.2. Model validation by protein manipulations

To further validate our proposed model and to illustrate the potential of the present model as a meaningful platform of

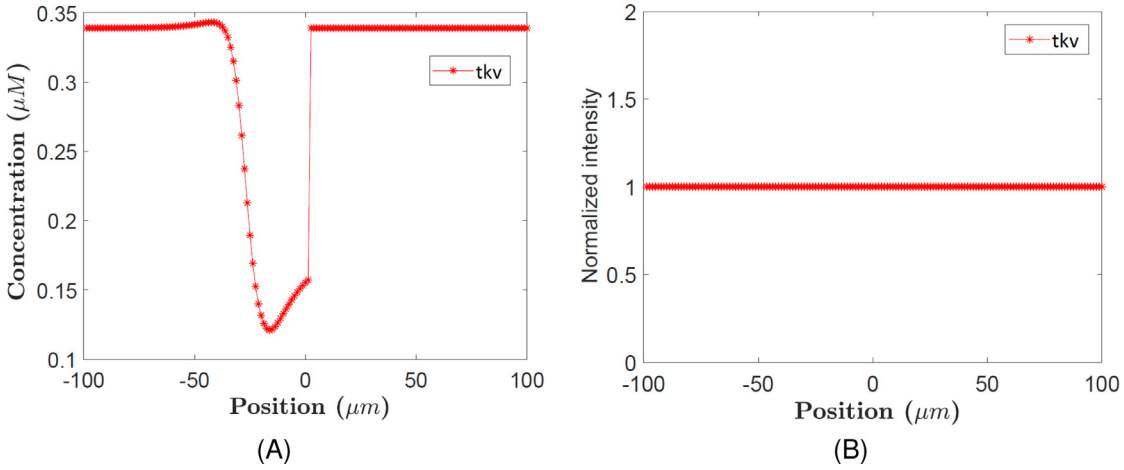

Fig. 7. Numerical profiles of *tkv* expression without the en upregulation (A) and Hh repression (B) in the presence of Dpp overexpression. (A)Computational profile of *tkv* expression without the en upregulation while overexpressing Dpp. (B)Numerical profile of *tkv* expression in the absence of En, Hh signaling and Dpp signaling where a uniform *tkv* expression distribution is obtained.

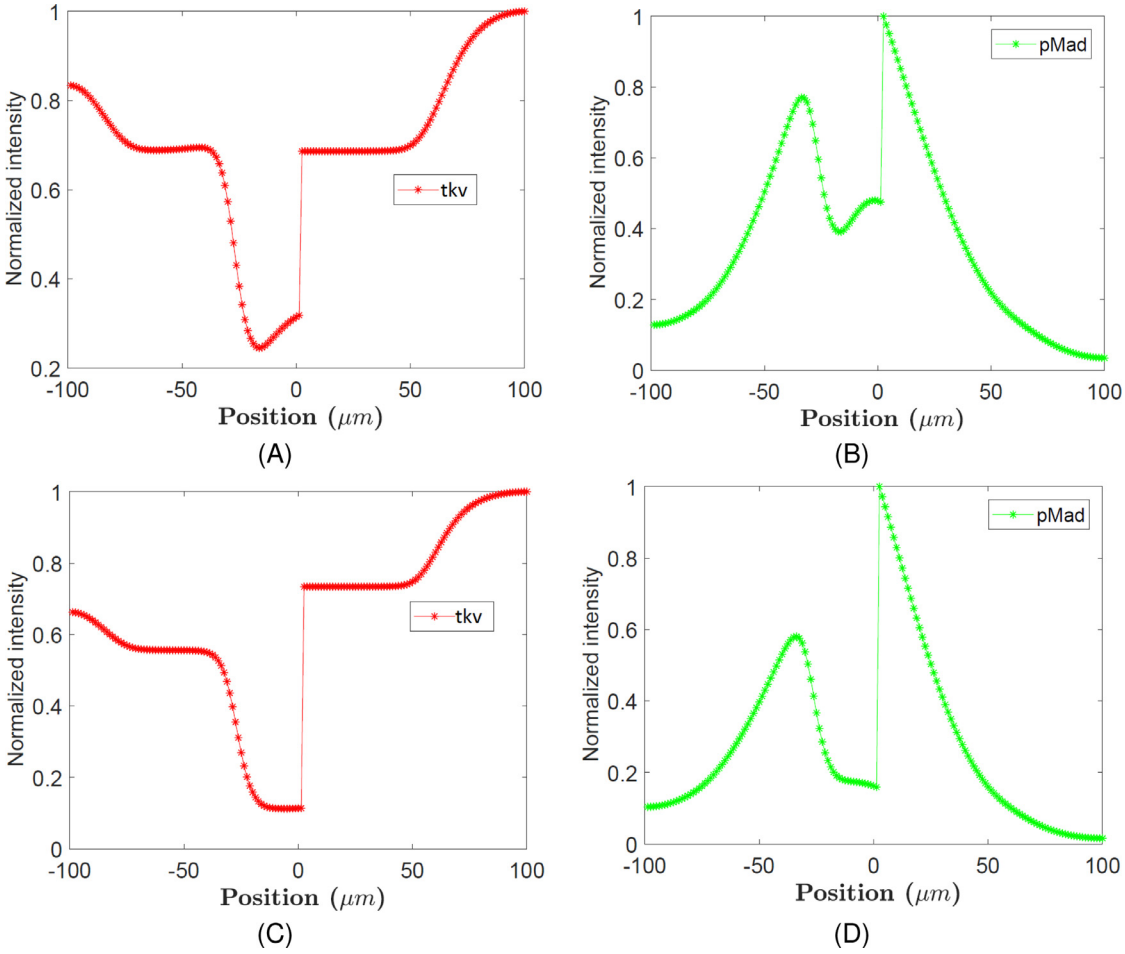

Fig. 8. Positive regulation of Tkv by Engrailed leads to a higher level of *tkv* expression in the P compartment than in the A compartment (A): The numerical pattern of *tkv* expression without the Engrailed (En) upregulation on Tkv by setting $r_{enp} = 0$; (B): The computational profile of pMad in the absence of the upregulation of Tkv by En; (C): The numerical pattern of *tkv* expression without the Engrailed (En) upregulation on Tkv in the A compartment by setting $r_{ena} = 0$; (D): Corresponding pMad with the upregulation of Tkv by En in the A compartment. In the absence of En-dependent upregulation in the P compartment, the higher level of *tkv* expression in the P compartment as shown in experimental observations (Tabata and Takei, 2004) disappears. Moreover, it is shown that without the En upregulation abutting the AP boundary, the lowest level of *tkv* expression, as well as the local minimum of pMad level in the central region, is shifted exactly to the AP boundary. Note that the normalized intensities of species in this and the following figures are obtained by dividing numerical concentration by the maximum computed concentration of corresponding species.

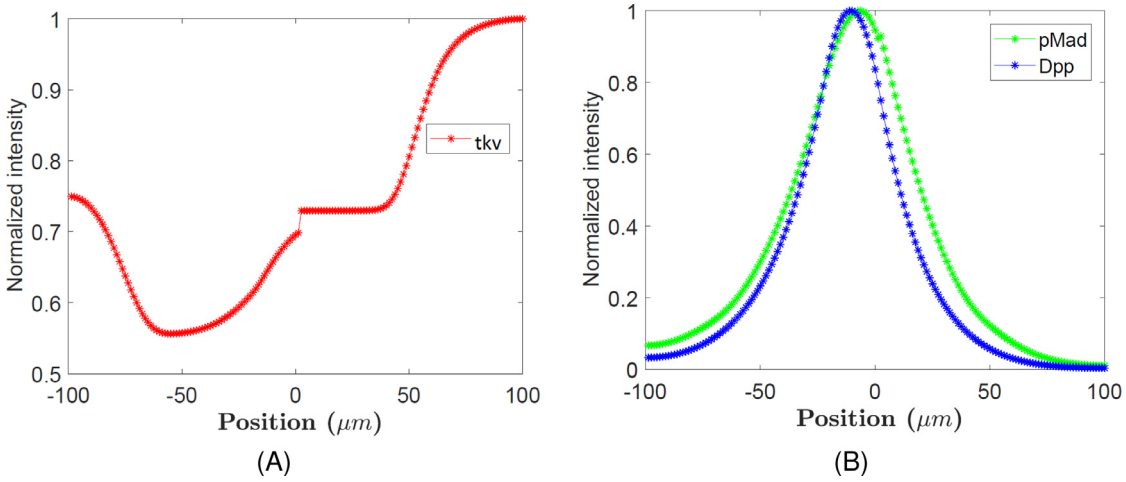

Fig. 9. Suppression of Tkv via Hh plays a critical role in the formation of complex *tkv* expression and pMad profiles. (A): The numerical pattern of *tkv* expression without the downregulation on Tkv by Hh via setting $r_{hhtkv} = 0$; (B): The corresponding computational profile of pMad in the absence of Hh repression. It is shown that without the repression by Hh signaling, not only the *tkv* expression distribution but also resulting pMad gradient changes dramatically. The hypersuppression of *tkv* expression at the AP boundary disappears. It results in the disappearance of the second peak of pMad in the A compartment and the shift of the global maximum of pMad. Note that the profile of Dpp displayed here is the numerical pattern of wild-type Dpp.

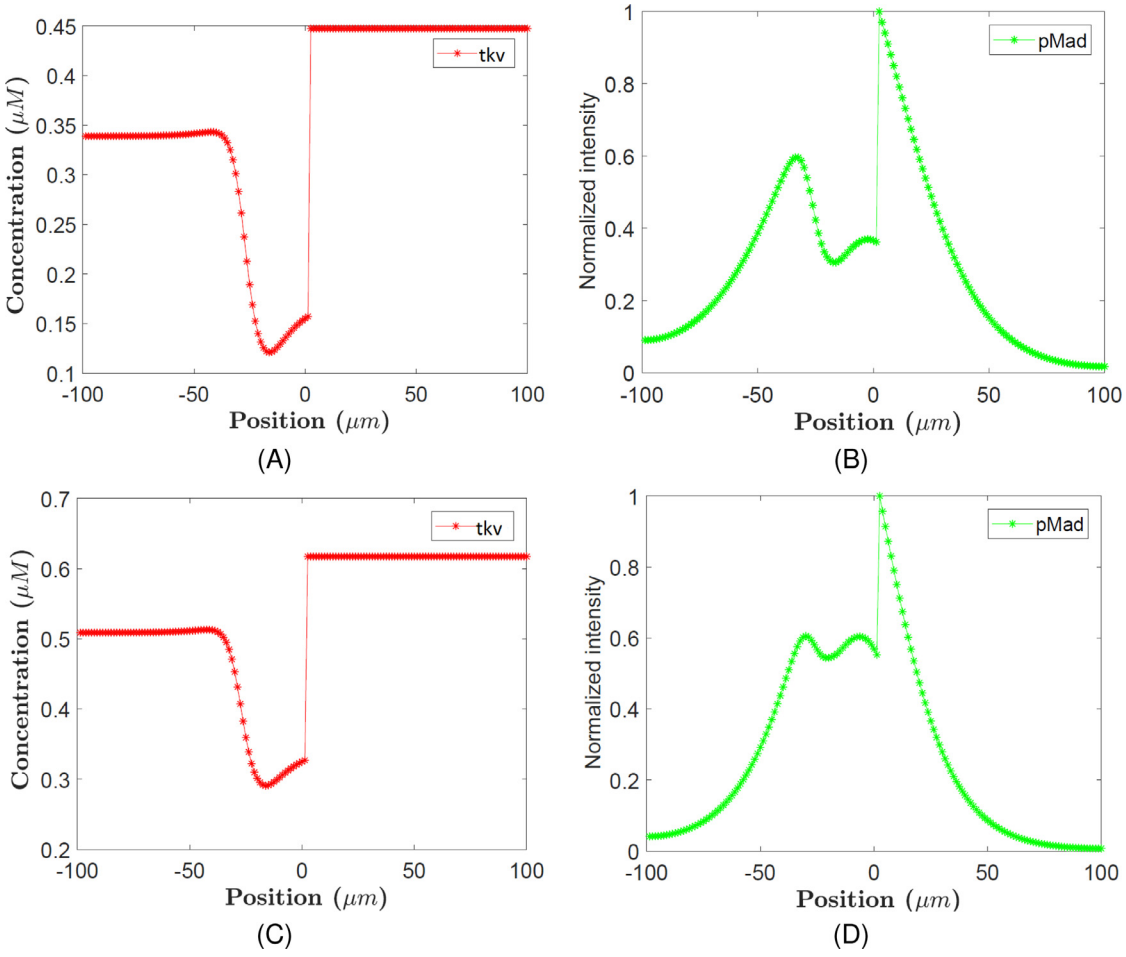

Fig. 10. Numerical profiles of *tkv* expression and pMad in both gene brk mutant (A,B) and brk overexpression (C,D). Here we set $\alpha_{brk} = 0$ in the model to mimic the *brk* mutant. It turns out that the profile of *tkv* expression in the *brk* mutant is the same as that in the presence of Dpp overexpression. In particular, the peripheral *tkv* expression is reduced to the basal level in both A and P compartments. In contrast, the hyperrepression of *tkv* expression remains at the AP boundary. Therefore, the overexpression of Dpp is equivalent to the *brk* mutant regarding their impact on the Tkv patterning. Our results suggest that Brk is involved in the process of Tkv repression by Dpp signaling. Moreover, To overexpress brk, we set $r_{pmd} = 0$ to remove the repression of Brk by pMad so that Brk can be overexpressed. It shows that with the overexpression of protein Brk, the basal Tkv is elevated to the peripheral level in both A and P compartments, so is the level in the hyperrepression region elevated. As a result, the pMad level is also clearly elevated in the central area and the pattern of pMad gradient changes in the region.

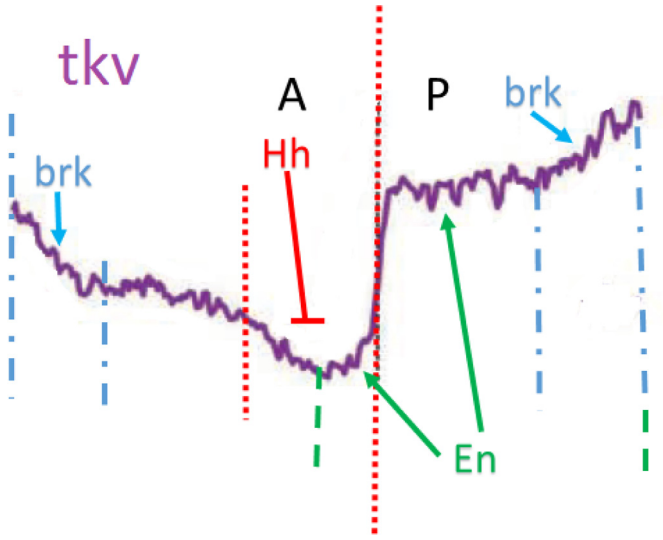

Fig. 11. Overview of how the highly asymmetrical pattern of *tkv* expression is established: Firstly, the short-range morphogen Hh downregulates the Tkv distribution at the central region where Hh induces the Dpp expression. Secondly, upregulation of the Tkv level by En generates a higher basal Tkv concentration in the P compartment than that in the A compartment. Meanwhile, the promotion of Tkv by En, which is induced by Hh, at the AP boundary locates the lowest Tkv level a few cell diameters away from the AP boundary. Thirdly, our model suggests that Brk significantly promotes the *tkv* expression in the peripheral regions. In other words, Dpp signaling negatively modulates the Tkv level by removing its downstream transcription factor Brk which positively regulates the Tkv in the medial region.

hypothesis test and mechanism examination, we repeated a couple of relevant manipulations from the literature using our model and compared with corresponding experimental observations. One is when Brk protein is greatly reduced, another is when *dpp* is over-expressed.

3.2.1. Brk mutations

Firstly, our model can reproduce the dramatic change of *brk* expression due to markedly reduced levels of Brk protein (Moser and Campbell, 2005). To see it, we set the Brk protein indicator T_{brk} to be 0 in order to represent Brk mutations. As a result, the manipulation leads to a fairly sharp boundary between high levels of expression laterally/mediolaterally while there is no expression medially. Further, the graded *brk* expression found in wild-type discs is lost. In addition, the *brk* level is substantially increased in the lateral regions where the level of *brk* expression is increased from 0.18 μM to 0.7 μM numerically. Our simulation outcome and experimental observation can be found in Fig. 5(C) and (D) in which it is clearly seen that our numerical result of Brk mutations is comparable with the experimental observations.

3.2.2. Overexpression of gene dpp

Secondly, our model is able to reproduce the dramatic changes of *tkv* expression and pMad profiles due to the overexpression of *dpp*. To investigate the role of Dpp in the patterning of Tkv, Tanimoto et al. monitored the distributions of *tkv* expression and pMad in discs that ubiquitously express dpp (Tanimoto et al., 2000). They found that (See Fig. 6(B)) (Tanimoto et al., 2000): (1) The level of peripheral *tkv* was significantly reduced to the basal level; (2) The basal level of *tkv* in the P compartment was still higher than in the A compartment; (3) The *tkv* level at the AP boundary remained hyperrepressed. Moreover, the pMad profile displays similar pattern (See Fig. 6(D)): (1) The distribution of pMad was ubiquitously elevated except at the AP boundary; (2) The level of pMad at the AP boundary was unchanged in the presence of Dpp overexpression; (3) The pMad level was higher in the P compartment than in the A compartment. To mimic the overexpression of Dpp, we set the Dpp level to be a constant throughout the whole domain by making $[Dpp]$ =0.2 μM. It turned out that our numerical predictions perfectly match the experimental outcomes and captures all the dramatic changes due to excess Dpp. The comparisons can be found in Fig. 6. In particular, the peripheral *tkv* is reduced to the basal level in both A and P compartments. In the A compartment, it is reduced from 0.42 μM to 0.34 μM which is our normal numerical basal level. Also, the *tkv* level is changed from 0.61 μM to 0.43 μM in the P compartment. In addition, the distribution of *tkv* remains hyperrepressed at the AP boundary in the anterior side. Regarding the pMad profile, it is also highly elevated in both of A and P compartment except for the AP boundary where the *tkv* distribution is hyperrepressed. In addition, the pMad level is still higher in the P compartment than that in the A compartment (0.29 μM vs 0.21 μM).

Therefore, Dpp signaling cannot be responsible for both the higher level of Tkv in the P compartment and the hyperrepression at the AP boundary. It has been postulated that the higher level of Tkv in the P compartment than that in the A compartment is purely caused by the positive regulation of Tkv by En, and the hyperrepression at the AP boundary is due to the repression by Hh signaling. To examine those hypotheses, we first turned off the En regulation terms in our model by setting $\alpha_{enp} = 0$ and $\alpha_{ena} = 0$ while keeping $[Dpp] = 0.2$ μM throughout the domain. It is seen in Fig. 7(A) that the basal level of *tkv* expression becomes the same in both A and P compartments, which indicates that the higher level of *tkv* expression in the P compartment can be completely attributed to En. Furthermore, we turned off the Hh repression term by making $r_{hhtkv} = 0$. Eventually, the hyperrepression at the AP boundary disappears as shown in Fig. 7(B), and the uniform distribution of *tkv* expression is displayed in the absence of En, Hh signaling, and Dpp signaling. Therefore, our model implies that the presence of En, Hh signaling, and Dpp signaling cooperate to establish the asymmetrical gradients of *tkv* expression and consequent pMad in the wing disc.

3.3. Roles of En, Hh signaling and Dpp signaling in the establishment of Tkv

In this section, we apply our validated model to examine individual roles of En, Hh signaling and Dpp signaling in the formation of complex profiles of Tkv and their impact on the Dpp signaling activity. In particular, the mechanism of Dpp-dependent repression of its receptor Tkv has been explored. By doing so, we may obtain a comprehensive view of the formation of Tkv gradient and then a better understanding of underlying mechanisms of the AP patterning in the Drosophila wing disc. Our testing factors include (i) upregulation of Tkv by En, (ii) Hh-dependent suppression of Tkv, and (iii) Brk-mediated repression of Tkv by Dpp signaling. All these analyses were conducted by manipulating individual functional terms in the model while keeping other parameter values unchanged.

3.3.1. Upregulation of Tkv by En

To show the effect of En, we first turned off the En upregulation term in the P compartment in Eq. (3) by setting $\alpha_{enp} = 0$. In the absence of En upregulation, one can not see a higher basal level of *tkv* expression in the P compartment than in the A compartment (See Fig. 8(A)). Note that all normalized intensities of species in the figures of the present work are obtained by dividing numerical concentrations by their maximum concentration. Moreover, quantitatively, the decay length of Dpp in the P compartment increases from 22.25 μm to 26.25 μm, and pMad decay length increases from 33.75 μm to 38.75 μm. Here the decay length of a species is calculated with the distance from the AP boundary to the position

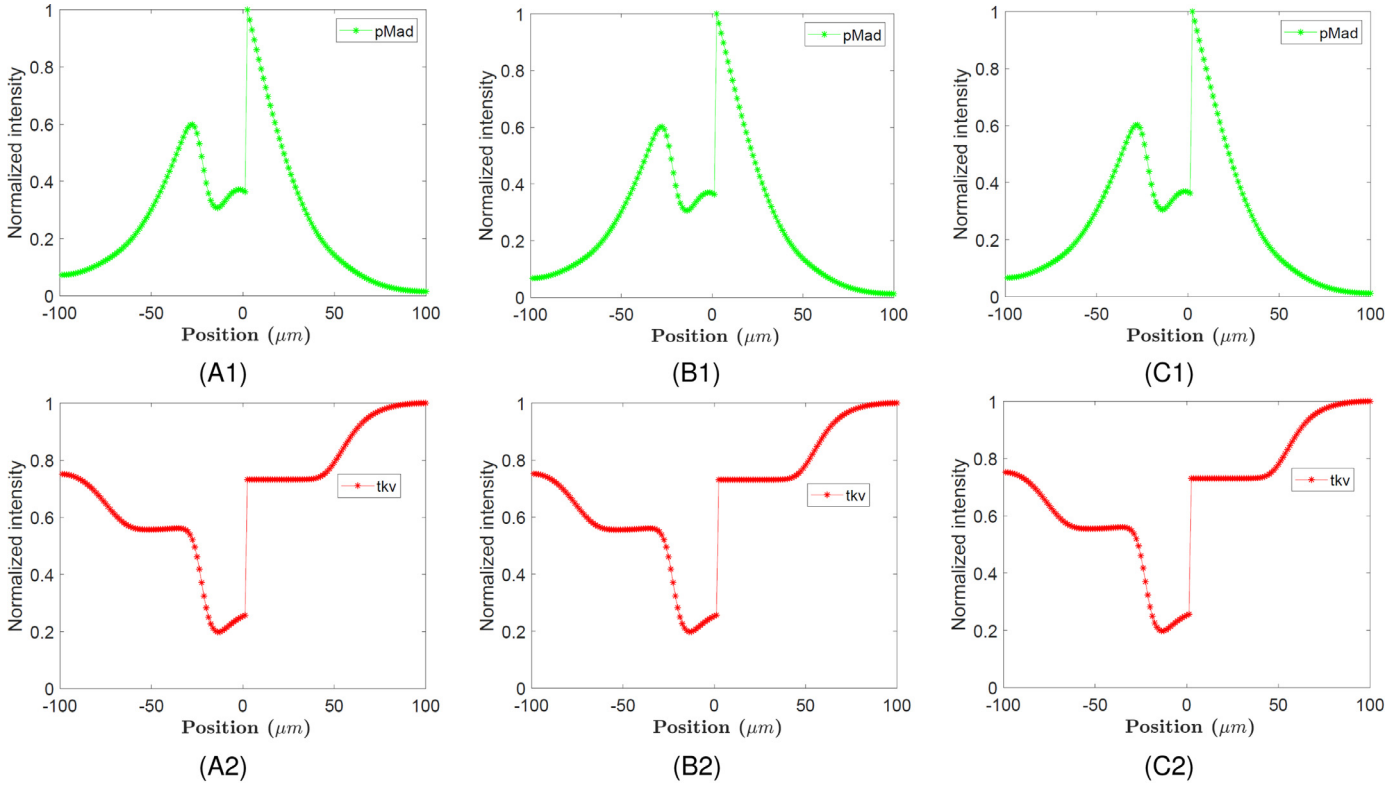

Fig. 12. Sensitivity of the system to the receptor/ligand binding rate k_{dt}^{+}. (A1) (B1)(C1) display the pMad profiles when $k_{dt}^{+} = 0.02\ \mu M^{-1}s^{-1}$, $k_{dt}^{+} = 0.1\ \mu M^{-1}s^{-1}$, and $k_{dt}^{+} = 3.2\ \mu M^{-1}s^{-1}$, respectively. (A2) (B2)(C2) show the tkv profiles when $k_{dt}^{+} = 0.02\ \mu M^{-1}s^{-1}$, $k_{dt}^{+} = 0.1\ \mu M^{-1}s^{-1}$, and $k_{dt}^{+} = 3.2\ \mu M^{-1}s^{-1}$, respectively. It turns out that with the value of k_{dt}^{+} changing over eightfold, the patterns of pMad and tkv level are maintained perfectly.

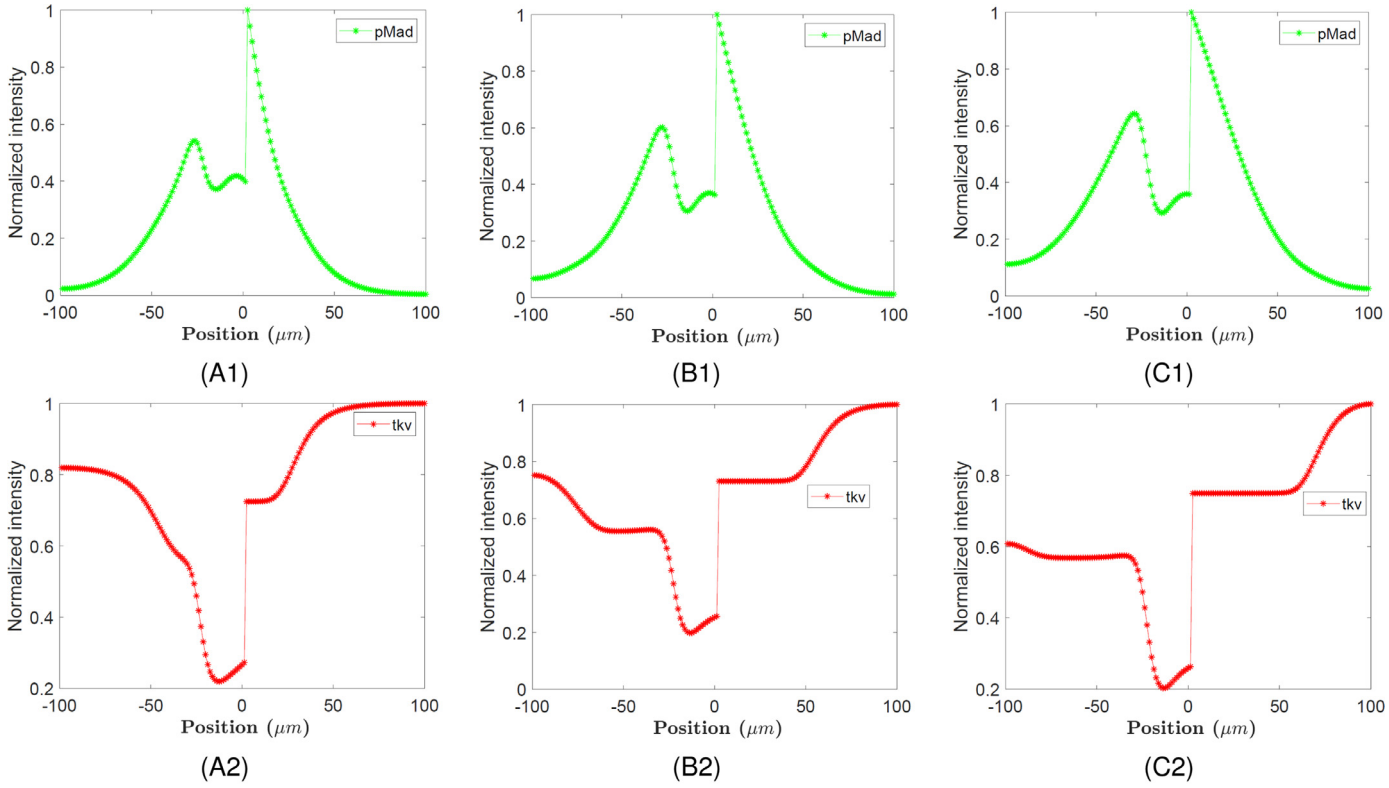

Fig. 13. Sensitivity of the system to Dpp diffusion coefficient D_{dpp}. (A1) (B1)(C1) display the pMad profiles when $D_{dpp} = 0.1\ \mu M^2/s$, $D_{dpp} = 0.3\ \mu M^2/s$, and $D_{dpp} = 0.5\ \mu M^2/s$, respectively. (A2) (B2)(C2) show the tkv profiles when $D_{dpp} = 0.1\ \mu M^2/s$, $D_{dpp} = 0.3\ \mu M^2/s$, and $D_{dpp} = 0.5\ \mu M^2/s$, respectively. The overall pattern of pMad is still quite robust against the change. However, some expected pattern changes of tkv expression are observed in the area away from the AP boundary due to the proposed mechanism that the Dpp signaling represses the tkv expression.

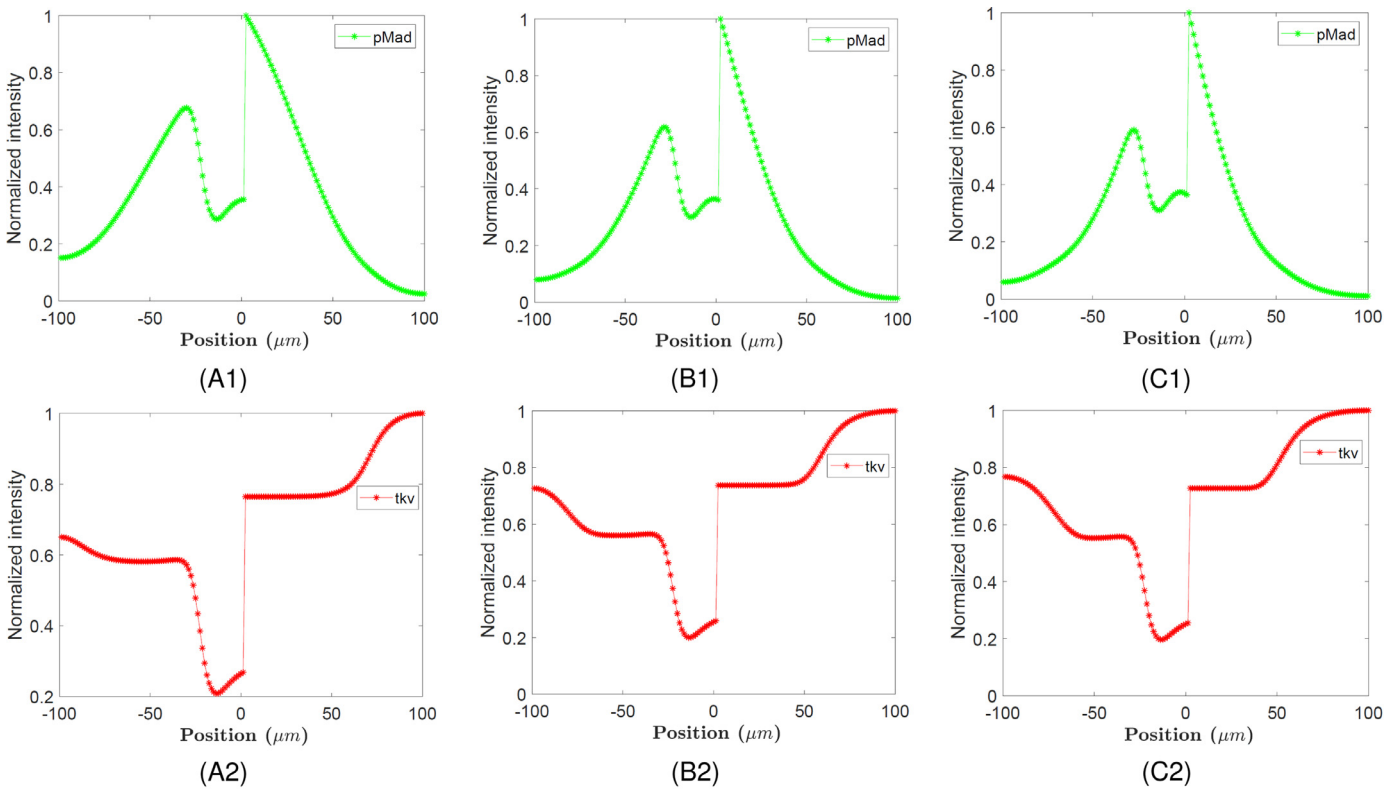

Fig. 14. Sensitivity of the system to degradation rate β_{dt}. (A1) (B1)(C1) display the pMad profiles when $\beta_{dt} = 1 \times 10^{-4}$ s^{-1}, $\beta_{dt} = 2 \times 10^{-4}$ s^{-1}, and $\beta_{dt} = 3 \times 10^{-4}$ s^{-1}, respectively. (A2) (B2)(C2) show the tkv profiles when $\beta_{dt} = 1 \times 10^{-4}$ s^{-1}, $\beta_{dt} = 2 \times 10^{-4}$ s^{-1}, and $\beta_{dt} = 3 \times 10^{-4}$ s^{-1}. It is observed that the patterns of pMad and tkv are also insensitive to the change except for some small changes of pMad and tkv in the peripheral regions.

where its concentration decays in the P compartment by a factor $\frac{1}{e}$ in comparison with the concentration level at the AP boundary. Therefore, it indicates that the promotion of Tkv by En in the P compartment mainly determines the higher level of Tkv in the area than that in the A compartment. As a result, the higher level of Tkv in the P compartment accounts for its steeper gradient of pMad since Tkv can trap Dpp via binding.

Moreover, it was shown experimentally that the lowest *tkv* expression level is located at the place a few cell diameters away from the AP boundary instead of precisely at the boundary (Tabata and Takei, 2004; Chen and Zou, 2018). To examine the cause, we shut down the En upregulation term in the A compartment in Eq. (3) by setting $\alpha_{ena} = 0$ only. In the absence of En upregulation, the lowest level of *tkv* expression, as well as the local minimum of pMad level in the central region, is shifted to the AP boundary. Therefore, our model suggests that the promotion of Tkv by En, induced by Hh signaling, makes the lowest *tkv* expression level a few cell diameters away from the AP boundary.

3.3.2. Hh-dependent suppression of Tkv

To examine the role of Hh-dependent suppression in the regulation of Tkv spatial distribution and corresponding Dpp signaling, we turned off the repression action of Hh signaling in Eq. (3) by setting $r_{hhtkv} = 0$ μM. It is seen in Fig. 9(A) that without the repression of Tkv by Hh, the hypersuppression of Tkv at the AP boundary does not exist anymore. The overall pattern of *tkv* expression gradient changes dramatically. Consequently, the pattern of pMad is surprisingly similar to the Dpp pattern (See Fig. 9(B)) even if the Tkv level is still under the control of En and Dpp signaling. In particular, the second peak of pMad in the A compartment disappears, and the global maximum peak shifts from the AP boundary to the peak position of Dpp level. Moreover, the decay length of Dpp in the P compartment decreases from 22.25 μm to 21.25 μm, and the pMad decay length decreases from 33.75 μm to 30.00 μm. Therefore, Hh signaling plays a critical role in the formation of complex *tkv* expression and pMad profiles. It also prevents the Dpp signaling from interfering and expands the effective range of Dpp signaling.

3.3.3. Brk-mediated repression of Tkv by Dpp signaling

As described in the introduction, the primary function of Dpp is to remove Brk from central regions of wing discs to allow for sal and omb expression (Campbell and Tomlinson, 1999). It is interesting to test whether the repression of Tkv by Dpp signaling is also through the removal of Brk in central regions. To the end, we have introduced the upregulation of Brk in the dynamics of *tkv* expression to represent the repression of Tkv by Dpp signaling in Eq. (4). A critical test is whether the Brk mutant leads to the same profile of *tkv* expression as that from the overexpression of Dpp in Section 3.2.2. Because Dpp signaling represses Brk, the overexpression of Dpp should be equivalent to the Brk mutant if Brk is involved in the repression process of Dpp signaling. To see it, we set $\alpha_{brk} = 0$ to mimic the *brk* mutant. It turns out that as predicted, the generated profile of *tkv* expression is the same as that reproduced in the situation of Dpp overexpression (See Figs. 10(A) and 6(A)). The peripheral *tkv* expression is reduced to the basal level in both A and P compartments. They are 0.34 μM and 0.43 μM in the A and P compartment, respectively. In contrast, the hyperrepression of *tkv* expression remains at the AP boundary. Moreover, the pMad pattern is surprisingly unchanged in the absence of Brk. The main reason is that the Dpp distribution is normal, the removal of increasing Brk distribution has no impact on the pMad level in the peripheral regions where there is normally no Dpp signaling.

Moreover, we did another manipulation to investigate the role of Brk in the establishment of Tkv gradient. The *brk* expression is numerically manipulated to be over-expressed by setting $r_{pmd} = 0$

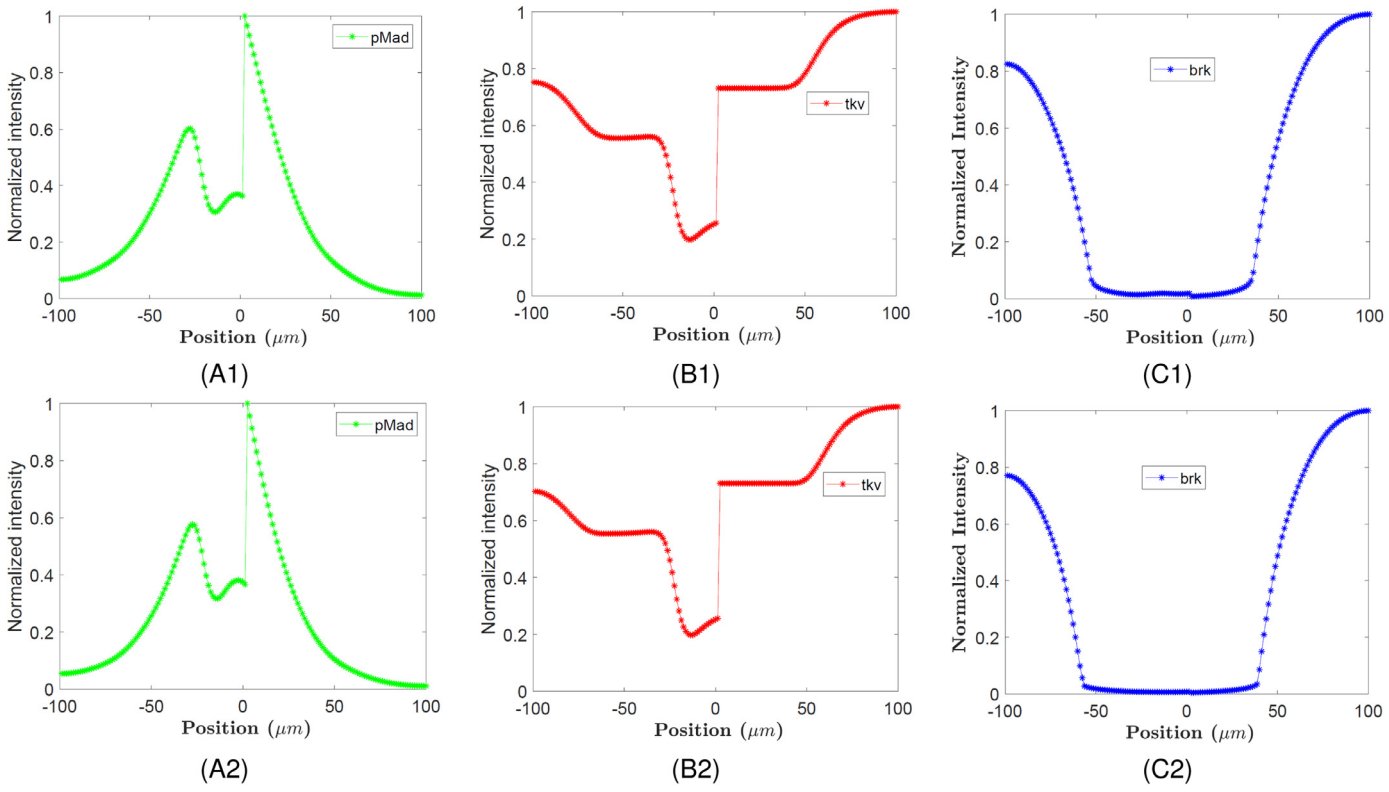

Fig. 15. A example of simultaneous parameter variation in the sensitivity analysis. (A1) (B1)(C1) show the profiles of pMad, tkv and brk expression, respectively when $D_{dpp} = 0.3\ \mu M^2/s, k_{dt}^{+} = 0.1\ \mu\ M^{-1}s^{-1}, \beta_{dt} = 2.52 \times 10^{-4}s^{-1}, \alpha_{tkv} = 8.57 \times 10^{-5}\ \mu M\ s^{-1}$. (A2) (B2)(C2) display the profiles of pMad, tkv and brk expression when $D_{dpp} = 0.6\ \mu M^2/s, k_{dt}^{+} = 3.2\ \mu M^{-1}s^{-1}, \beta_{dt} = 4 \times 10^{-4}s^{-1}, \alpha_{tkv} = 1.7 \times 10^{-4}\ \mu M\ s^{-1}$. It illustrates that our computed patterns are quite robust against simultaneous changes of multiple parameters within their reasonable range.

which removes the repression of *brk* by pMad. As a result, the *brk* level becomes constant everywhere. With the overexpression of Brk, the basal Tkv is elevated to the peripheral level in both A and P compartments. Fig. 10(C) displays the numerical *tkv* expression profile when overexpressing Brk. In the A compartment, it is increased from 0.34 μM to 0.42 μM. And the basal *tkv* expression level is elevated from 0.43 μM to 0.61 μM in the P compartment. Besides, the distribution of *tkv* expression is increased from 0.12 μM to 0.3 μM in the hyperrepression area at the AP boundary. Consequently, the pMad level is also elevated in the central region, which changes its original pattern of two peaks (see Fig. 10(D)). Therefore, our model suggests that most likely Brk mediates the Dpp-dependent repression of Tkv. To repress the *tkv* expression, Dpp only needs to remove *brk* activity via pMad.

4. Conclusion

Decapentaplegic (Dpp) signaling is essential for both patterning and growth in the wing disc. The Dpp major type-I receptor Tkv is indispensable for Dpp signaling. In this paper, we focused on theoretically investigating mechanisms by which the highly asymmetric pattern of Tkv gradients is established in the Drosophila wing disc. In particular, inspired by the fact that a large number of Dpp signaling activities is through the transcription factor Brk, we proposed that Brk also mediates the Dpp-dependent repression of Tkv which leads to a sharp increase of the Tkv distribution in the peripheral regions. To test the idea, we extended a previous baseline model of the AP patterning by incorporating a new equation of Brk into our model and adding the promotion of Brk into the Tkv equation. It has been shown that our proposed mathematical model is able to accurately reproduce complex profiles of *tkv* expression, pMad and *brk* expression throughout the wing disc. As a digital experimental platform, our model also enables us to reproduce *tkv* expression and pMad distributions in the cases of *brk* gene mutants and Dpp overexpression.

Moreover, the present model, which integrates several important experimental observations, allows us to test hypotheses and provide a relatively comprehensive view of the formation of the highly asymmetric pattern of the Tkv gradient. We found that En, Hh signaling, and Dpp signaling all play an essential role in establishing the complex experimentally-observed patterns of *tkv* expression and Dpp signaling activity indicated by pMad. An illustration of contributors to the *tkv* expression gradient at different regions of wing disc is displayed in Fig. 11. First of all, the short-range morphogen Hh greatly downregulates the Tkv distribution in the central region where Hh induces Dpp gene expression. As a result, it expands the effective range of Dpp gradient and prevents the Dpp signaling from interfering Hh signaling. Secondly, upregulation of the Tkv level by En generates a higher basal Tkv concentration in the P compartment than that in the A compartment. It leads to both a steeper gradient of pMad and a shorter effective range of Dpp in the P compartment. Meanwhile, the promotion of Tkv at the AP boundary by En locates the lowest Tkv level a few cell diameters away from the AP boundary. Thirdly, our model suggests that Dpp signaling negatively modulates the Tkv level by removing its downstream transcription factor Brk, which positively regulates Tkv. By doing so, Dpp facilitates its spreading at the central region. Moreover, the increasing level of Brk in the peripheral regions significantly contributes to the sharp increase of the Tkv distribution in the area.

It has been previously shown that Brk can mediate many Dpp signaling activities such as the induction of Dpp target genes (Campbell and Tomlinson, 1999; Winter and Campbell, 2004) and growth control (Doumpas et al., 2013). In this work, we

proposed that that Brk also mediates the repression of Dpp receptor Tkv. In future work, to test the Brk-mediated mechanism of Dpp-dependent repression of Tkv, we may work with biologists to mimic *brk* mutants and *dpp* overexpression, which are described in Section 3.3.3, and observe the corresponding profiles of *tkv* expression and pMad in the lab. Moreover, currently, the mechanism by which Brk positively regulates the gene *tkv* expression is not well understood. It is not known if Brk upregulates the *tkv* expression directly or indirectly (del Álamo Rodrıguez et al., 2004). The mechanism of how Brk upregulates Tkv will be investigated in our further model development and analysis.

Acknowledgments

The author gives special thanks to Dr. Hans G. Othmer of the University of Minnesota for past invaluable support which led to author's great interest in theoretical studies of patterning and growth in the Drosophila wing imaginal disc. The author also would like to thank the anonymous reviewers, Dr. Dongyu Jia (Department of Biology) and Dr. Yuting Zou (Department of Mathematical Sciences) of Georgia Southern University for their constructive comments and suggestions to improve the manuscript quality. This work was supported in part by National Science Foundation grant DMS-1818748.

Appendix A

A1. The Hh module (Chen and Zou, 2018)

$$\frac{\partial [Hh]}{\partial t} = D_{hh}\frac{\partial^2 [Hh]}{\partial x^2} + (1-a(x))\alpha_{enhh} - k_{hp}^{+}[Hh][ptc] + k_{hp}^{-}[\overline{HP}] - \beta_{hh}[Hh] \tag{6}$$

$$\frac{\partial [Ptc]}{\partial t} = a(x)\alpha_{Ptc} + \alpha_{sigptc}\frac{[Signal]^p}{(M_{Ptc})^p + [Signal]^p} - k_{hp}^{+}[Hh][Ptc] + k_{hp}^{-}[\overline{HP}] - \beta_{Ptc}[Ptc] \tag{7}$$

$$\frac{\partial [\overline{HP}]}{\partial t} = -k_{hp}^{-}[\overline{HP}] + k_{hp}^{+}[Hh][Ptc] - \beta_{hp}[\overline{HP}] \tag{8}$$

$$\frac{\partial [Signal]}{\partial t} = \alpha_{signal}\frac{\left(\frac{[\overline{HP}]}{[Ptc]}\right)^s}{(M_{signal})^s + \left(\frac{[\overline{HP}]}{[Ptc]}\right)^s} - \beta_{signal}[Signal] \tag{9}$$

where $[Hh]$, $[Ptc]$ and $[\overline{HP}]$ are concentrations of Hh, Ptc, and the Hh-Ptc complex, respectively. The variable [Signal] is introduced for the concentration of Hh signaling activity so that the intensity to activate the Hh target gene expressions is simply reflected by the level of [Signal]. Here there is not a particular molecular mechanism about how the Hh-Ptc complex and Ptc produce intracellular signaling activity. Regarding the parameter notations, D_{hh} is the diffusion coefficient for Hh; k_{hp}^{+} represents the association rate of the Hh-Ptc complex; k_{hp}^{-} is taken as corresponding dissociation coefficient. $\beta_{(\cdot)}$ is used for rates of degradation. a(x) is a characteristic function of the A compartment in which $a(x) = 1$ in the A compartment and $a(x) = 0$ in the P compartment.

A2. Proof that tkv expression level is proportional to the level of total Tkv proteins

If we have the gene *tkv* in the model system, all regulations (positive and negative) of Tkv will be upon the gene *tkv*. Then we may have three equations as the following to describe the levels of gene *tkv* expression [*tkv*], free Tkv protein [*Tkv*]) and Bound Tkv protein[$\overline{DT}$], respectively:

$$\frac{\partial [tkv]}{\partial t} = = \alpha'_{tkv} + (1-a(x))\alpha'_{enp} + \alpha'_{ena}\frac{\left(\frac{[\overline{HP}]}{[Ptc]}\right)^{ne}}{(M_{en})^{ne} + \left(\frac{[\overline{HP}]}{[Ptc]}\right)^{ne}} - r'_{hhtkv}\frac{\left(\frac{[\overline{HP}]}{[Ptc]}\right)^{nh}}{(M_{hp})^{nh} + \left(\frac{[\overline{HP}]}{[Ptc]}\right)^{nh}} + \alpha'_{bt}\frac{[brk]^{nb}}{M_{brk}^{nb} + [brk]^{nb}} - \beta'_{tkv}[tkv] \tag{10}$$

$$\frac{\partial [Tkv]}{\partial t} = T_{tkv}[tkv] - k_{dt}^{+}[Dpp][Tkv] + k_{dt}^{-}[\overline{DT}] - \beta_{tkv}[Tkv] \tag{11}$$

$$\frac{\partial [\overline{DT}]}{\partial t} = k_{dt}^{+}[Dpp][Tkv] - k_{dt}^{-}[\overline{DT}] - \beta_{dt}[\overline{DT}] \tag{12}$$

Where $\alpha'_{tkv} = \alpha_{tkv}/T_{tkv}$, $\alpha'_{ena} = \alpha_{tkv}/T_{tkv}$, $\alpha'_{enp} = \alpha_{enp}/T_{tkv}$, $r'_{hhtkv} = r_{hhtkv}/T_{tkv}$, $\alpha'_{bt} = \alpha_{bt}/T_{tkv}$ are all regulation rates, and T_{tkv} represents the translation rate from gene *tkv* to protein Tkv. Addition of Eq. (11) and Eq. (2) leads to the following equation for the rate of change of total Tkv protein level.

$$\frac{\partial [Tkv]}{\partial t} = T_{tkv}[tkv] - \beta_{tkv}[Tkv] - \beta_{dt}[\overline{DT}] \tag{13}$$

When $\beta_{tkv} \approx \beta_{dt}$, at the equilibrium state we have

$$[tkv] = \frac{\beta_{tkv}}{T_{tkv}}([\overline{DT}] + [Tkv])$$

The above process shows that it is reasonable to assume that the gene *tkv* expression level is proportional to the level of total Tkv protein which consists of [$\overline{DT}$] and [*Tkv*].

A3. Positivity of Tkv *concentration at steady state*

At steady state, by setting $\frac{\partial [\overline{DT}]}{\partial t} = 0$ in Eq. (2), we have

$$[\overline{DT}]_{ss} = \frac{k_{dt}^{+}[Dpp]_{ss}[Tkv]_{ss}}{k_{dt}^{-} + \beta_{dt}} \tag{14}$$

Here sub index *ss* is used to represent the steady-state solutions of involved species. Then plugging the formula (14) into Eq. (3) and making $\frac{\partial [Tkv]}{\partial t} = 0$ leads to

$$[Tkv]_{ss} = \frac{NR}{\frac{k_{dt}^{+}[Dpp]_{ss}}{k_{dt}^{-} + \beta_{dt}} + \beta_{tkv}} \tag{15}$$

Where

$$NR = \alpha_{tkv} + (1-a(x))\alpha_{enp} + \alpha_{ena}\frac{\left(\frac{[\overline{HP}]_{ss}}{[Ptc]_{ss}}\right)^{ne}}{(M_{en})^{ne} + \left(\frac{[\overline{HP}]_{ss}}{[Ptc]_{ss}}\right)^{ne}}$$

$$-r_{hhtkv}\frac{\left(\frac{[\overline{HP}]_{ss}}{[Ptc]_{ss}}\right)^{nh}}{(M_{hp})^{nh}+\left(\frac{[\overline{HP}]_{ss}}{[Ptc]_{ss}}\right)^{nh}}+\alpha_{bt}\frac{[brk]_{ss}^{nb}}{M_{brk}^{nb}+[brk]_{ss}^{nb}}$$

Therefore, it is clear that if $\alpha_{tkv}-r_{hhtkv}>0$, $NR>0$ and then $[Tkv]_{ss}>0$ based on formula (15) in which $[Dpp]_{ss}>0$ and the values of all involved parameters are positive.

A4. Parameters estimation

Parameters values in the Hh module are taken from previous sound estimates (Nahmad and Stathopoulos, 2009). Readers can refer to those papers and related supporting material for biological references. Parameter values in the Dpp signaling module were either extracted from the literature or estimated according to empirical or experimental measurements. First of all, some core parameters were decided and their values were determined. Then other remaining parameters were calculated either from the literature or based on a specific relationship between some of the core parameters and individual parameters. Those relationships were derived according to particular acceptable experimental measurements at a steady state such as Dpp decay length measured by Kicheva et al. (2007) Finally, a base set of all parameter values was chosen for our wild-type computation and reported in Tables 1 and 2. Their detailed estimate processes and related supporting literature are described in the following:

Diffusion Coefficients A simple formulation can provide a starting point for the diffusion estimation of mobile species in terms of the molecular weight M, temperature T and solution viscosity μ (Young et al., 1980)

$$D=8.34*10^{-8}\left(\frac{T}{\mu M^{1/3}}\right)\quad cm^2s^{-1} \tag{16}$$

With Eq. (16), one can calculate that the green fluorescent protein (GFP), a 238 amino acid and 27 KDa protein, has a sound diffusion coefficient of 85 μm^2 s^{-1} in water by assuming 1cP for the viscosity of water and 298 K for temperature *T*. However, the cytoplasm is considerably more viscous than water under the same temperature, roughly by a factor of 10. As such, Lander et al. used 10 μm^2 s^{-1} for the Dpp diffusion coefficient in their numerical simulations (Lander et al., 2002). Moreover, if the adjustment for tissue tortuosity is taken into consideration, the diffusion can be 4–5 fold lower than that without the tissue tortuosity (Lander et al., 2002). Furthermore, when it involves impacts from the binding to immobile extracellular matrix molecules, binding to membrane receptors, and endocytosis, the restricted diffusion can be further slower. Therefore, by considering diffusion and degradation of Dpp only in a wing disc and aided with experimental measurements, Kicheva et al. estimated the effective diffusion coefficient of GFP-Dpp to be 0.1 ± 0.05 μm^2 s^{-1} (Kicheva et al., 2007). Since the binding to membrane receptors is explicitly considered in our model, our effective diffusion coefficients should be bigger than 0.1 μm^2 s^{-1}. Based on the above considerations, 0.3 μm^2 s^{-1} is set as a base value in our computations for Dpp effective diffusion coefficient.

Degradation rates It was biochemically measured that the extracellular Dpp molecules in the Drosophila wing discs are degraded almost entirely within 3 hours (Teleman and Cohen, 2000). As such, the degradation rate of Dpp should be greater than 10^{-4} s^{-1}. With the aid of a computational model, Kicheva et al. estimated that Dpp was degraded at a rate $\beta_{dt}=2.52\times10^{-4}s^{-1}\pm1.29\times10^{-4}$ s^{-1} which corresponds to a GFP-Dpp half-life of about 45 minutes which is consistent with the turnover time of Dpp in the developing wing (Kicheva et al., 2007). In the present work and others (Lander et al., 2005), it is assumed that Dpp degradation is receptor-driven. Because of it, the degradation rate of Dpp-Tkv complex should be comparable to the degradation rate of Dpp. Therefore, we set $\beta_{dt}=2.52\times10^{-4}$ s^{-1} as its base value which is similar to what was used in other numerical work (Lander et al., 2002; 2005). In addition, we set $\beta_{tkv}=\beta_{dt}=2.52\times10^{-4}s^{-1}$ assuming that bound and unbound Tkv have the same degradation rate.

Kinetic binding parameters For the binding affinity k_{dt}^{+}, we set 0.1 μ M^{-1} s^{-1} as its base value. 0.1 μ M^{-1} s^{-1} was estimated by Lander et al. for the Dpp association rate to obtain an acceptable maximum of receptors per cell (Lander et al., 2002). It was also used by Nahmad et al. for the association of Hh and its receptor Ptc (Nahmad and Stathopoulos, 2009).

Moreover, k_{dt}^{-} is estimated in a way that the numerical decay length of Dpp can be consistent with the experimental measurement by Kicheva et al. (2007). The measured decay length is 20.2 ± 5.7 μm in the P compartment. The following is our computational process of k_{dt}^{-}: First of all, considering that the concentration of a measured functional GFP-Dpp in the Kicheva's work actually equals to the summation of the concentrations of free Dpp and its complex $\overline{DT}$ in our work, we combined Eqs. (1) and (2) to have

$$\frac{\partial[Dpp+\overline{DT}]}{\partial t}=D_{dpp}\frac{\partial^2[Dpp]}{x^2}-\beta_{dt}[\overline{DT}] \tag{17}$$

According to Eq. (2), at equilibrium state

$$[\overline{DT}]=\frac{k_{dt}^{+}}{k_{dt}^{-}+\beta_{dt}}[Dpp][Tkv]\approx C_{dt}[Dpp] \tag{18}$$

where $C_{dt}=\frac{k_{dt}^{+}}{k_{dt}^{-}+\beta_{dt}}[Tkv]_{\max}$. Here we assumed that in the P compartment where the decay length was experimentally-measured, the concentration of Tkv can be roughly regarded as a constant. The constant is similar to the maximum receptor level of Tkv $[Tkv]_{\max}$ in the A compartment which is estimated in the next paragraph. This assumption is supported by experimental observations that Tkv levels do not change dramatically in the P compartment and that the basal Tkv level in the P compartment is comparable to the maximum level of Tkv in the A compartment (See Fig. 1). Then plugging (18) into Eq. (17) yields

$$\frac{\partial[Dpp]}{\partial t}=\frac{D_{dpp}}{1+C_{dt}}\frac{\partial^2[Dpp]}{x^2}-\frac{\beta_{dt}C_{dt}}{1+C_{dt}}[Dpp] \tag{19}$$

This leads to a formula of decay length γ of Dpp

$$\gamma=\sqrt{\frac{D_{dpp}}{\beta_{dt}C_{dt}}} \tag{20}$$

From Eq. (20), k_{dt}^{-} is calculated as

$$k_{dt}^{-}=\frac{\gamma^2\beta_{dt}k_{dt}^{+}[Tkv]_{max}}{D_{dpp}} \tag{21}$$

By using the values of $\beta_{dt}, k_{dt}^{+}, [Tkv]_{\max}, D_{dpp}$ and experimentally-measured $\gamma=20.2$ μm, one has $k_{dt}^{-}\approx0.0067$ s^{-1}.

Maximum levels of Dpp and receptor Tkv It was measured by Kicheva et al. (2007) that the maximum level of Dpp at the source boundary is $\rho=4379\pm1741$ molecules per cell. Based on this measurement, we obtained $[Dpp]_{\max}\approx0.90$ μM by a conversion formula $[Dpp]=\frac{\rho}{VN_A}$ in which N_A is Avogadro constant 6.022×10^{23} and $V\approx\frac{4}{3}\pi(2.5/2)^3=8.18$ μm^3. Moreover, the maximum receptor level of Tkv in the wing disc system was estimated at 1600 molecules per cells (Nahmad and Stathopoulos, 2009; Lander et al., 2002). With the same unit conversion, it is equivalent to 0.34 μM which was taken as our $[Tkv]_{\max}$.

Maximal activation rate At the place where the maximum level of Dpp occurs, the net production of Dpp should be maximized, and the diffusion effects can be ignored. As such, from the Eq. (1) at the steady state, one has in the position of maximum Dpp level:

$$\alpha_{dpp} = k_{dt}^{+}[Dpp]_{max}[Tkv] - k_{dt}^{-}[DT]$$

$$= k_{dt}^{+}[Dpp]_{max}[Tkv] - \frac{k_{dt}^{-}k_{dt}^{+}}{k_{dt}^{-}+\beta_{dt}}[Dpp]_{max}[Tkv] \quad (22)$$

$$= \frac{k_{dt}^{+}\beta_{dt}}{(k_{dt}^{-}+\beta_{dt})}[Dpp]_{max}[Tkv] \quad (23)$$

Moreover, we set the concentration $[Tkv] = c_l[Tkv]_{\max}$ at the position of maximized Dpp. Here c_l is a small number (we set it equal to 0.2 in our computation) since the Tkv level is much lower in the position than the maximum value (Tabata and Takei, 2004). Plugging the related parameter values into Eq. (22) gives us $\alpha_{dpp} = 2 \times 10^{-4}$ μM s^{-1}.

To estimate the ubiquitous activation rate α_{tkv}, we chose a place far away from the AP boundary in the A compartment to get rid of Hh and Dpp repressions, En upregulation and interactions with Dpp. Then at steady state, Eq. (3) becomes

$$\alpha_{tkv} = \beta_{Tkv}[Tkv]_{max}$$

In addition, α_{en}, which is used to model the En upregulation of the Tkv (Tabata and Takei, 2004), is set as $\alpha_{en} = \frac{4}{5}\alpha_{tkv}$. The coefficient $\frac{4}{5}$ was approximated according to the experimentally measured profile (see Fig. 1) in which the maximum level of Tkv in the P compartment is much higher than the maximum level in the A compartment but less than twofold. Finally, through numerical trials, we set Hh repression rate $r_{hhtkv} = \frac{2}{5}\alpha_{tkv}$ and $r_{dpptkv} = 2\alpha_{tkv}$ to make $[Tkv]$ very low in the Hh signaling cells as shown in experimental profiles (Tabata and Takei, 2004).

Some other related parameters We set $d = p = 3$, $nh = 3.4$ and $M_{hp} = M_{signal} = 2.135$ as used in the Nahmad's model (Nahmad and Stathopoulos, 2009) for the Hh signaling network. Moreover, the half maximal activation parameter M_{dpp} should be smaller than M_{Ptc} since the expression of gene *dpp* is induced with a much lower threshold than gene *ptc* (Tabata and Takei, 2004; Ayers et al., 2010). Here $M_{dpp} = 0.05$ μM $< M_{Ptc} = 0.14$ μM in our computation. Parameters associated with the equation of brk are set to be comparable to those used for other species. For instance, $\alpha_{brk} = r_{pmad} = 3 \times 10^{-5}$ μM $s^{-1} \approx \alpha_{ena} = 2.74 \times 10^{-5}$ μM s^{-1}, and $ne, nb \in (1, 6.8)$.

A5. Parameter sensitivity analysis and model robustness

As described in the above section of parameter estimation, we selected some key parameters to form a base core set which includes diffusion coefficient, receptor/ligand binding parameters, and degradation. In fact, even for those parameters in the core set, the range of biologically plausible values may span over several-fold change or even several orders of magnitude in the literature. For instance, the diffusion coefficients of Dpp morphogen between 0.1 μm^2 s^{-1} and 80 μm^2 s^{-1} were used (Lander et al., 2002; Kicheva et al., 2007); The range of degradation rate spans from 10^{-4} s^{-1} to 5×10^{-3} s^{-1} (Teleman and Cohen, 2000; Kicheva et al., 2007; Nahmad and Stathopoulos, 2009); And the association rates varying from 0.01 μM $^{-1}$ s^{-1} to 16 μ M^{-1} s^{-1} were considered to be plausible (Umulis et al., 2006; Lander et al., 2002).

Therefore, it is worthwhile to check whether our proposed model is robust against parameter changes and to find out whether our results or conclusions are restricted to specific choices of parameter values. To the end, we addressed the parameter sensitivity using a method called one-factor-at-a-time (OFAT) as our primary approach. In particular, one variable is changed at a time while all other variables are kept fixed. Then comparisons among numerical results (before and after changes) are carried out. Note that in this work we focus on the qualitative similarity of patterns for important species such as tkv expression, pMad, and brk expression. OFAT is one of the simplest and most common approaches for sensitivity analysis in mathematical modeling. Modelers frequently prefer it due to some practical reasons. For example, it appears to be a logical approach since any change observed in the output can unambiguously be due to the change of a single variable. So it increases the comparability of the results. Moreover, it minimizes the chances of computer program crashes which more likely occur when one changes several input factors simultaneously. In additional to OFAT, the simultaneous variation of input variables is also considered in our analysis.

Firstly, we evaluated the sensitivity of our model system to the changes of associated parameters by the OFAT approach. We found that our model is robust against parameter variations within their reasonable range. Here the detailed analysis is only shown for some key parameters in the core set including the receptor/ligand binding rate k_{dt}^{+}, the diffusion coefficient of Dpp D_{dpp}, and the Dpp degradation rate β_{dt}. To analyze the sensitivity to k_{dt}^{+}, we varied it over eightfold from 0.02 $\mu M^{-1}s^{-1}$ to 3.2 $\mu M^{-1}s^{-1}$. It exhibits that the patterns of pMad and tkv are very robust against the change of k_{dt}^{+}. With the value of binding rate changing over eightfold, the patterns are maintained perfectly as indicated in Fig. 12. Moreover, when the diffusion coefficient of Dpp D_{dpp} is changed from 0.1 $\mu M^2/s$ to 0.7 $\mu M^2/s$. As seen in Fig. 13, the overall pattern of pMad is still quite robust against the change, while some expected pattern changes of tkv expression are observed in the area away from the AP boundary. In particular, if D_{dpp} is relatively smaller (or larger), less (or more) Dpp molecules diffuse to peripheral regions. It causes less (or more) Dpp signaling in the areas. Consequently, the concentration of tkv expression increases faster (or slower) since the Dpp signaling represses the activation of tkv expression as our model proposes. In addition, we calculated the sensitivity of the system to the Dpp degradation rate β_{dt}. It is observed that the patterns of pMad and tkv are also insensitive to the change of β_{dt} within the range between 1.0×10^{-4} s^{-1} to 4.0×10^{-4} s^{-1} except for some small changes of pMad and tkv in the peripheral regions. The explanation is that larger (or smaller) Dpp degradation rate results in the less (or more) Dpp signaling. As a result, it leads to a faster (slower) increase of tkv concentration in the areas because of that Dpp signaling suppresses the tkv expression. The sensitivity against Dpp degradation is displayed in Fig. 14. Therefore, our conclusions are not restricted to specific choices of parameter values. Some results of parameter sensitivity analysis can even contribute to (or be predicted by) our conclusions.

Secondly, we performed the sensitivity analysis with the simultaneous variation of parameters. It is evident that our model is still robust to the simultaneous parameter changes. For instance, the profiles of pMad, tkv expression and brk expression are not visibly changing when one varies simultaneously Dpp effective diffusion coefficient D_pp from 0.3 $\mu M^2/s$ into 0.6 $\mu M^2/s$, receptor/ligand binding rate k_{dt}^{+} from 0.1 $\mu M^{-1}s^{-1}$ into 3.2 $\mu M^{-1}s^{-1}$, degradation rate β_{dt} from 2.52×10^{-4} s^{-1} into 4.0×10^{-4} s^{-1}, tkv production rate from 8.57×10^{-5} μM s^{-1} into 1.7×10^{-4} μM s^{-1}. The comparison of patterns can be seen in Fig. 15. Note that due to numerous combinations of simultaneous variation, other numerical results are not shown here.

References

del Álamo Rodrıguez, D., Felix, J.T., Dıaz-Benjumea, F.J., 2004. The role of the t-box gene optomotor-blind in patterning the drosophila wing. Dev.Biol. 268 (2), 481–492.

Ayers, K.L., Gallet, A., Staccini-Lavenant, L., Thérond, P.P., 2010. The long-range activity of hedgehog is regulated in the apical extracellular space by the glypican dally and the hydrolase notum. Dev.Cell 18 (4), 605–620.
Bangi, E., Wharton, K., 2006. Dpp and gbb exhibit different effective ranges in the establishment of the BMP activity gradient critical for drosophila wing patterning. Dev. Biol. 295 (1). 178–93
Ben-Zvi, D., Pyrowolakis, G., Barkai, N., Shilo1, B., 2011. Expansion-repression mechanism for scaling the dpp activation gradient in drosophila wing imaginal discs.
Campbell, G., Tomlinson, A., 1999. Transducing the dpp morphogen gradient in the wing of drosophila: regulation of dpp targets by brinker. Cell 96 (4), 553–562.
Casali, A., Struhl, G., 2004. Reading the hedgehog morphogen gradient by measuring the ratio of bound to unbound patched protein. Nature 431 (7004), 76–80.
Chen, Z., Zou, Y., 2018. Anterior-posterior patterning of Drosophila wing discs I: an baseline mathematical model. submitted
Doumpas, N., Ruiz-Romero, M., Blanco, E., Edgar, B., Corominas, M., Teleman, A.A., 2013. Brk regulates wing disc growth in part via repression of myc expression. EMBO Rep. 14 (3), 261–268.
Funakoshi, Y., Minami, M., Tabata, T., 2001. mtv shapes the activity gradient of the Dpp morphogen through regulation of thickveins. Development 128 (1), 67.
Hamaratoglu, F., Affolter, M., Pyrowolakis, G., 2014. Dpp/bmp signaling in flies: from molecules to biology. In: Seminars in Cell & Developmental Biology, 32. Elsevier, pp. 128–136.
Irons, D.J., Wojcinski, A., Glise, B., Monk, N.A., 2010. Robustness of positional specification by the Hedgehog morphogen gradient. Dev. Biol. 342, 180–193.
Kicheva, A., Pantazis, P., Bollenbach, T., Kalaidzidis, Y., Bittig, T., Julicher, F., Gonzalez–Gaitan, M., 2007. Kinetics of morphogen gradient formation. Science 315 (5811), 521–525.
Lander, A.D., Nie, Q., Wan, F.Y., 2002. Do morphogen gradients arise by diffusion? Dev. Cell 2 (6). 785–96
Lander, A.D., Nie, Q., Wan, F.Y.M., 2005. Spatially distributed morphogen production and morphogen gradient formation. Math.Biosci.Eng. (2) 239–262.
Lecuit, T., Cohen, S.M., 1998. Dpp receptor levels contribute to shaping the dpp morphogen gradient in the *Drosophila* wing imaginal disc.. Development 125, 4901–4907.
Moser, M., Campbell, G., 2005. Generating and interpreting the Brinker gradient in the Drosophila wing. Dev.Biol. 286 (2), 647–658.
Nahmad, M., Stathopoulos, A., 2009. Dynamic interpretation of hedgehog signaling in the drosophila wing disc. PLoS Biol. 7 (9), e1000202.
Pandey, U.B., Nichols, C.D., 2011. Human disease models in drosophila melanogaster and the role of the fly in therapeutic drug discovery. Pharmacol.Rev. 63 (2), 411–436.
Restrepo, S., Zartman, J.J., Basler, K., 2014. Coordination of patterning and growth by the morphogen dpp. Curr. Biol. 24 (6), R245–R255.
Shimizu, K., Gurdon, J.B., 1999. A quantitative analysis of signal transduction from activin receptor to nucleus and its relevance to morphogen gradient interpretation. Proc. Natl. Acad. Sci. 96 (12), 6791–9796.
Strigini, M., Cohen, S.M., 1997. A hedgehog activity gradient contributes to AP axial patterning of the drosophila wing. Development 124, 4697–4705.
Tabata, T., Takei, Y., 2004. Morphogens, their identification and regulation. Development 131 (4). 703–12
Tanimoto, H., Itoh, S., ten Dijke, P., Tabata, T., 2000. Hedgehog creates a gradient of DPP activity in Drosophila wing imaginal discs. Mol. Cell 5 (1), 59–71.
Teleman, A.U., Cohen, S.M., 2000. Dpp gradient formation in the *drosophila* wing imaginal disc. Cell 103 (6), 971–980.
Umulis, D.M., Othmer, H.G., 2015. The role of mathematical models in understanding pattern formation in developmental biology. Bull.Math.Biol. 77 (5), 817–845.
Umulis, D.M., Serpe, M., O'Connor, M.B., Othmer, H.G., 2006. Robust, bistable patterning of the dorsal surface of the drosophila embryo. Proc. Natl. Acad. Sci. U S A 103 (31). 11613–8
Winter, S.E., Campbell, G., 2004. Repression of dpp targets in the drosophila wing by brinker. Development 131 (24), 6071–6081.
Young, M., Carroad, P., Bell, R., 1980. Estimation of diffusion coefficients of proteins.. Biotechnol. Bioeng. 22.